

advances.sciencemag.org/cgi/content/full/6/35/eabb4591/DC1

Supplementary Materials for

The NEMP family supports metazoan fertility and nuclear envelope stiffness

Yonit Tsatskis, Robyn Rosenfeld, Joel D. Pearson, Curtis Boswell, Yi Qu, Kyunga Kim, Lacramioara Fabian, Ariz Mohammad, Xian Wang, Michael I. Robson, Karen Krchma, Jun Wu, João Gonçalves, Didier Hodzic, Shu Wu, Daniel Potter, Laurence Pelletier, Wade H. Dunham, Anne-Claude Gingras, Yu Sun, Jin Meng, Dorothea Godt, Tim Schedl, Brian Ciruna, Kyunghee Choi, John R. B. Perry, Rod Bremner, Eric C. Schirmer, Julie A. Brill, Andrea Jurisicova*, Helen McNeill*

*Corresponding author. Email: mcneillh@wustl.edu (H.M.); jurisicova@lunenfeld.ca (A.J.)

Published 28 August 2020, *Sci. Adv.* **6**, eabb4591 (2020)
DOI: 10.1126/sciadv.abb4591

This PDF file includes:

- Figs. S1 to S8
- Tables S1 and S2
- Supplementary Materials and Methods
- References

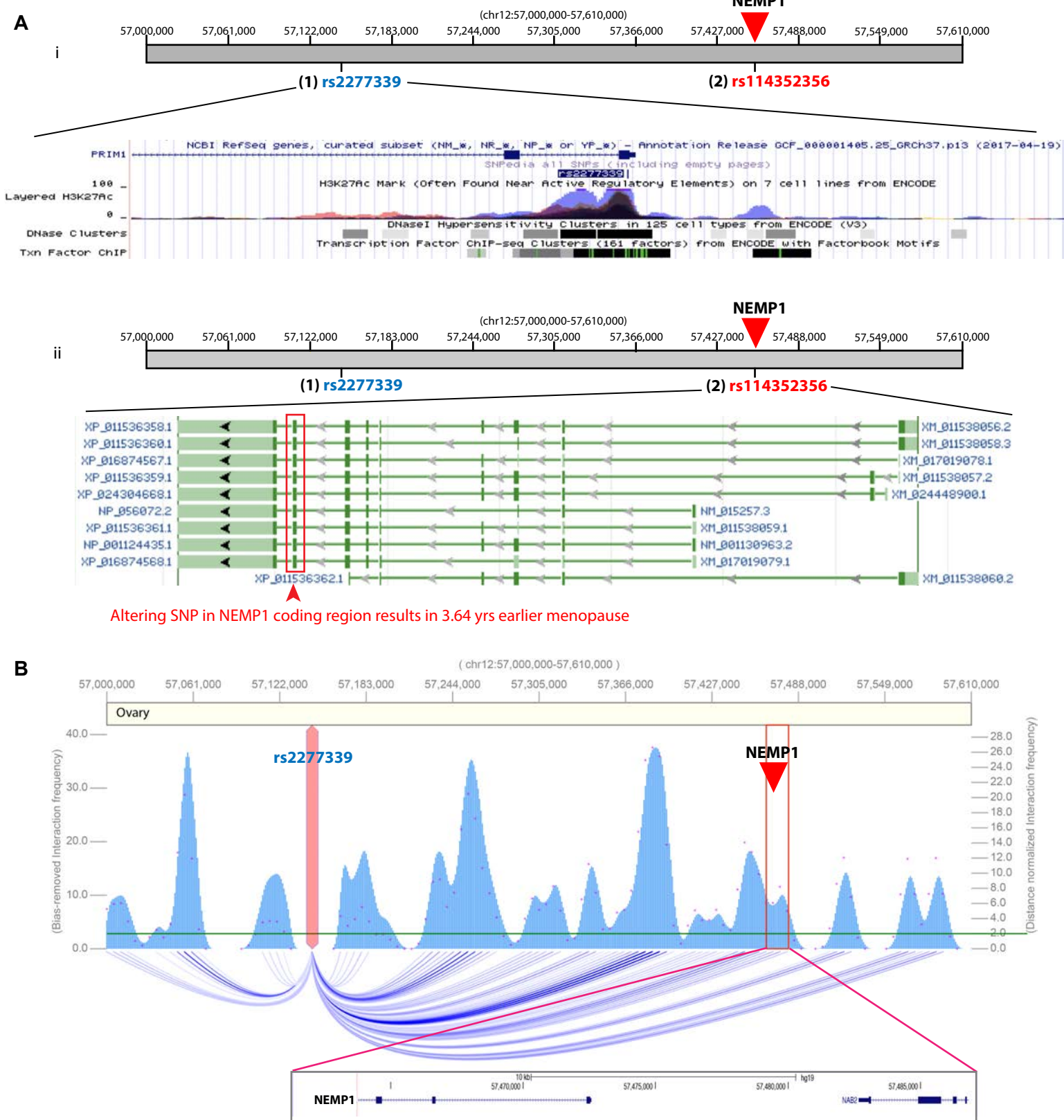


fig. S1. NEMP1 associated GWAS SNPs and human ovary HiC. (A) SNPs found near and within the *NEMP1* locus are associated with reduced age at menopause. (i) SNP rs2277339 is found 300kb upstream of *NEMP1*. H3k27Ac (a classic enhancer mark), as well as DNase accessibility (open chromatin) are consistent with rs2277339 acting as an enhancer region. (ii) SNP rs114352356 which lies within the *NEMP1* locus is associated with 3.6yrs earlier menopause. (B) Human ovary long range interaction (HiC) data using Hg19 reference genome shows physical interactions between rs2277339 and *NEMP1*. Data processed and analysed by 3DIV: A 3D-genome interaction viewer and database. Inset: Hg19 reference genome, snapshot from UCSC genome browser of area boxed in grey.

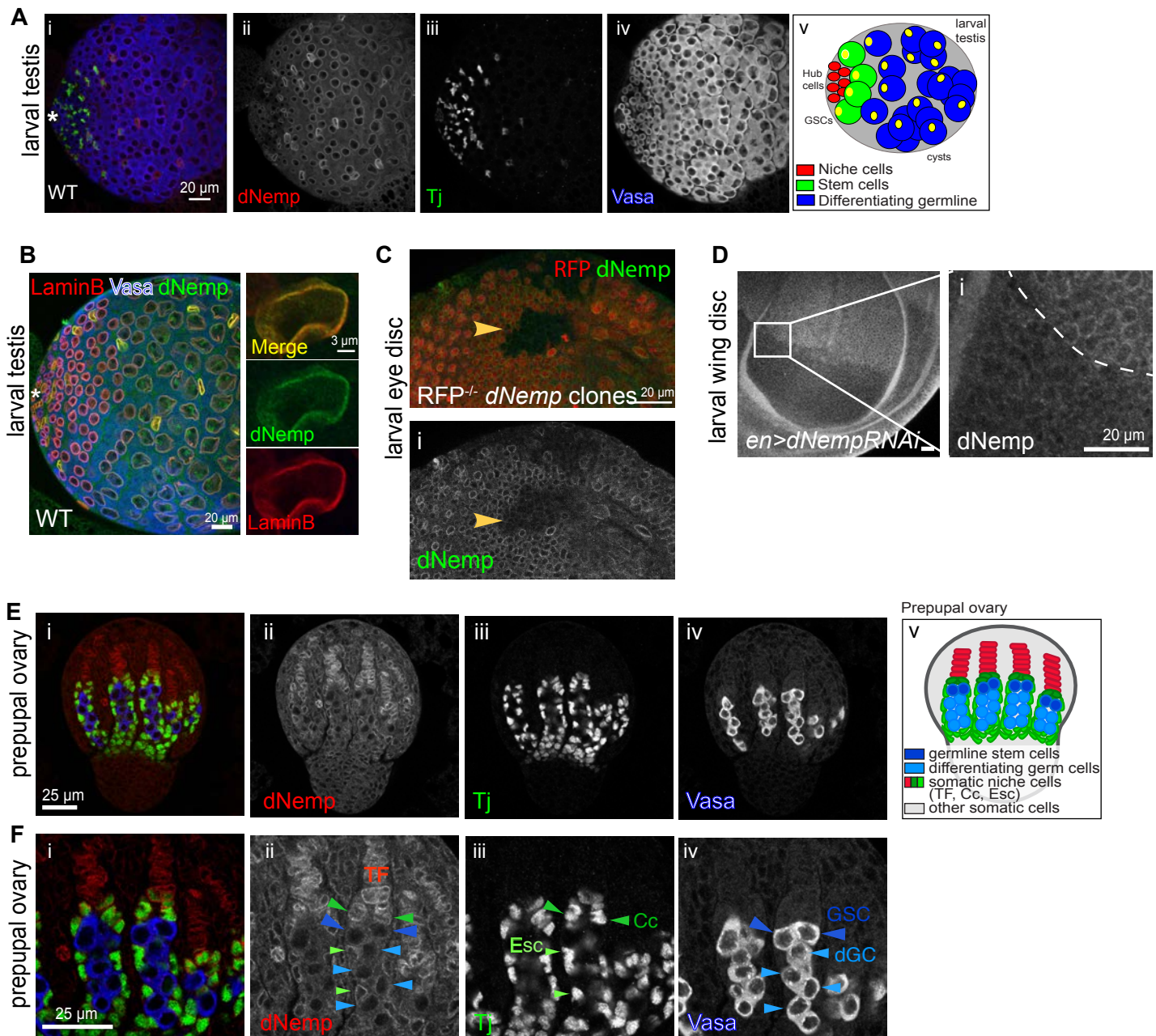


fig. S2. Nemp localization and antibody verification. (A) Nemp is expressed in both germline and somatic cells in the *Drosophila* testes. WT *Drosophila* testis stained with anti-dNemp antibody (ii), early cyst cell marker Traffic jam (Tj) (iii) and germ cell marker Vasa (iv). Hub of the testis is marked by an asterisk. Schematic of larval testis depicted in (v). (B) dNemp is expressed on the nuclear envelope of germ cells in the *Drosophila* testes. Larval testis stained for dNemp, LaminB and Vasa. Single germ cell nucleus viewed on the right. (C) Validation of dNemp antibody, showing that dNemp is reduced in *dNemp*^{-/-} null larval eye clones. dNemp staining (green, i) is strongly reduced in *dNemp*^{-/-} null larval eye clones. Lack of RFP marks mutant tissue (yellow arrowhead). (D) Further validation of dNemp antibody specificity and effectiveness of the knock-down. Reduction in dNemp protein levels (i) in the anterior of a larval wing disc expressing *enGal4>dNemp* RNAi. Dotted line denotes anterior/posterior boundary of the wing. dNemp is reduced in the *enGal4* expressing half of the eye. (E) Expression of dNemp in WT prepupal *Drosophila* ovary showing expression in both somatic and germline cells. Ovary stained with anti-dNemp antibody (ii), Tj, which is expressed by somatic cells contacting the germline cells (iii), and germ cell marker Vasa (iv). dNemp is ubiquitously expressed. Schematic of prepupal ovary depicted in (v). (F) Magnification of (E). TF, terminal filament (red). Arrowheads point to escort cells (Esc, light green), cap cells (Cc, dark green), germline stem cells (GSC, dark blue), and differentiating germ cells (dGC, light blue).

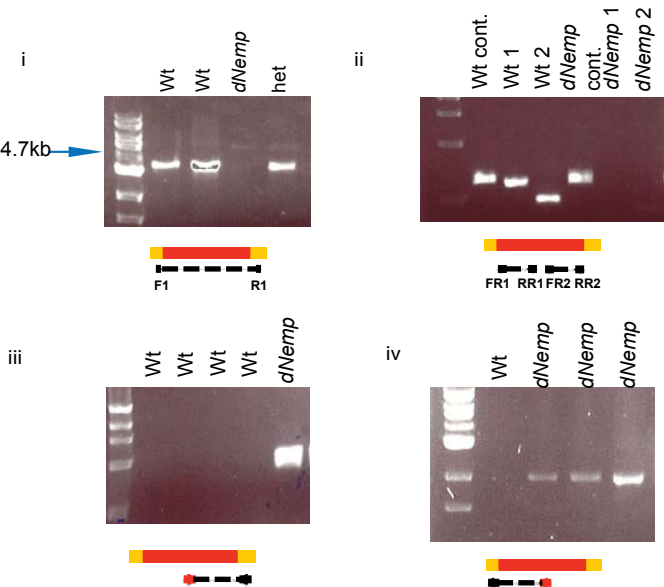
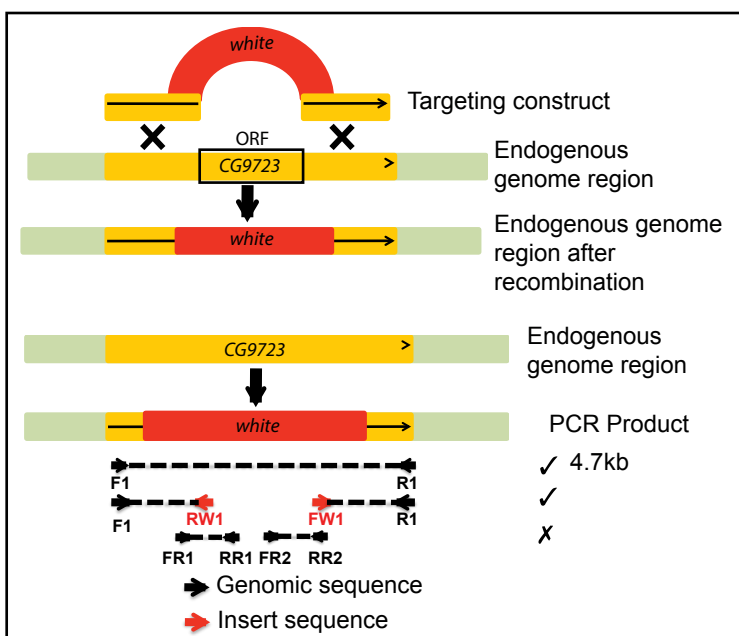
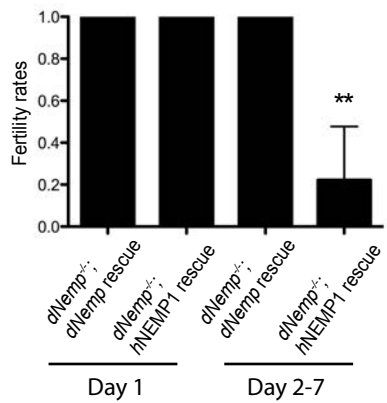
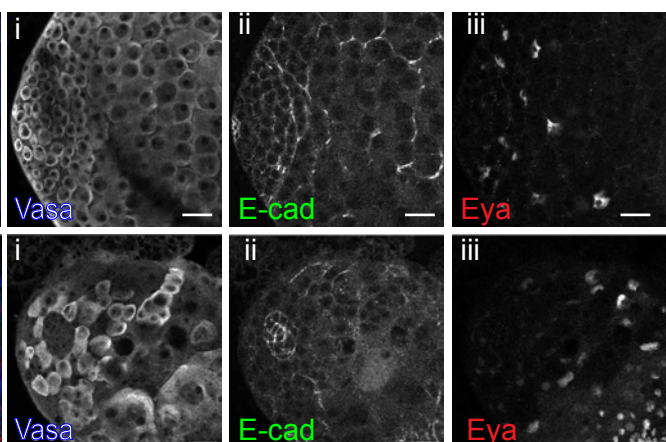
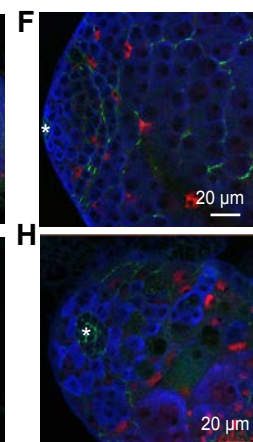
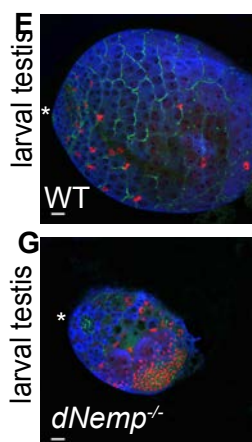
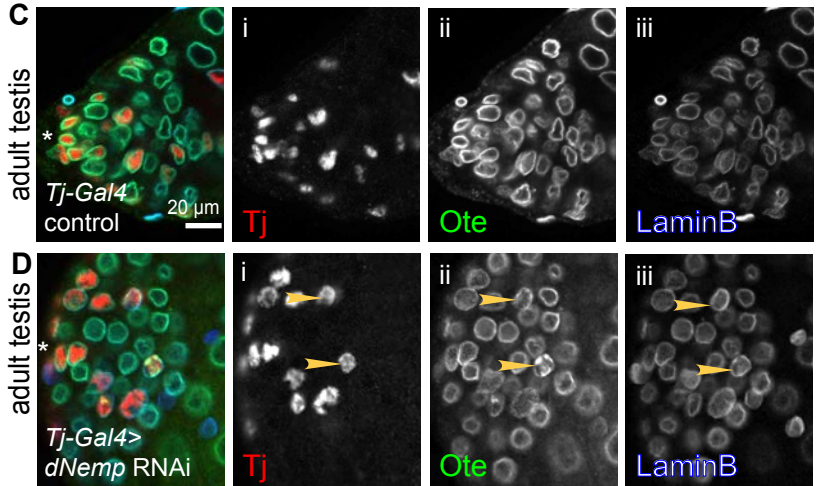
A**B****C**

fig. S3. Generation of *dNemp*^{-/-} null alleles and defects in *Drosophila* testes. (A) Genetic strategy to generate a *dNemp*^{-/-} null mutant through ends-out recombination. (i-iv) Single flies were tested with PCR for absence of the coding region of *dNemp* and the correct placement of the *white* gene replacing the *dNemp* codons, followed by sequencing validation. (B) Sperm exhaustion of *dNemp*^{-/-} males rescued with *tubulinGal4* driven-*dNemp* or -*hNEMPI* that eclosed on Day 1 or on subsequent days (Day 2-7). Single males were mated to three WT females for three days beginning on the day of their eclosure for *dNemp*^{-/-}; *dNemp* rescue ($n=7$) and *dNemp*^{-/-}; *hNEMPI* rescue ($n=6$) for day 1 eclosure and for *dNemp*^{-/-}; *dNemp* rescue ($n=41$) and for *dNemp*^{-/-}; *hNEMPI* rescue ($n=26$) for days 2-7 eclosure. *hNEMPI* rescue flies eclosing on days 2-7 were significantly less fertile than *dNemp* rescue flies. (C-D) Knockdown of *dNemp* in cyst cells leads to NE defects. Adult testes stained with *Tj* (red, i), *Ote* (green, ii) and *LaminB* (blue, iii). By comparison to *Tj-Gal4* control (C), *Tj-Gal4>dNemp* RNAi testes display a mislocalization of *Otefin* while *LaminB* is largely unaffected (yellow arrowheads) in cyst cells (D). (E-H) Immunostaining for *Vasa* demonstrating presence of early germ cells (i), *DE-cadherin* (E-cad) showing loss of cyst cell integrity (ii), and *Eyes absent* (Eya) revealing normal transition to cyst cell fate (iii) at low (E, G) and high (F, H) magnification in WT (E, F) and *dNemp*^{-/-} (G, H) testes.

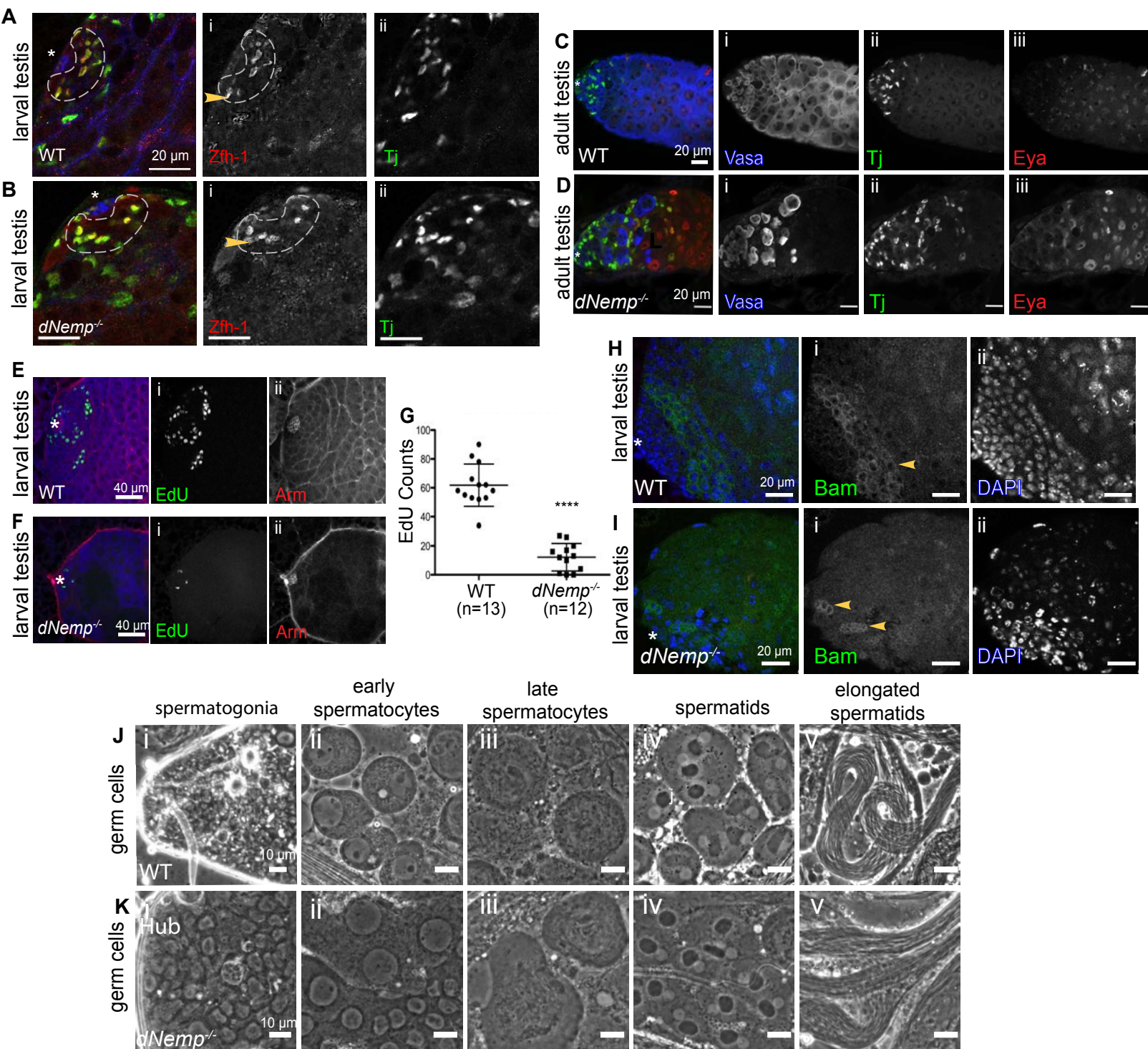


fig. S4. Characterization of testis defects in *dNemp* mutants. (A-B) WT (A) and *dNemp^{-/-}* (B) larval testes showing cyst stem cells are present in mutants as indicated by Zfh-1 (yellow arrowheads). Region including stem cells are marked by dotted line. Cyst cells go through normal fate transitions as indicated by attaining Tj expression. (C-D) In WT, germ cells are organized and Tj cells transition into Eya cells. In *dNemp^{-/-}* testes, Tj cells still differentiate into Eya cells indicating normal fate progression in cyst cell differentiation. (E-G) Larval testes of WT (E) and *dNemp^{-/-}* mutants (F) stained with proliferation marker EdU (i) and Arm (ii). (G) Corresponding EdU counts showing reduction of proliferation in *dNemp^{-/-}* mutant larval testes. (H-I) The germline factor Bag-of-marbles (Bam) can be seen as a continuous band in the apical region of WT testes (H), however, it is only detected in a few clusters of cells (yellow arrowheads) in *dNemp^{-/-}* testes (I). (J-K) Phase contrast images of developing male germ cells: (i) spermatogonia, (ii) early spermatocytes, (iii) late spermatocytes, (iv) spermatids, and (v) elongated spermatids from (J) WT and (K) *dNemp^{-/-}* mutants.

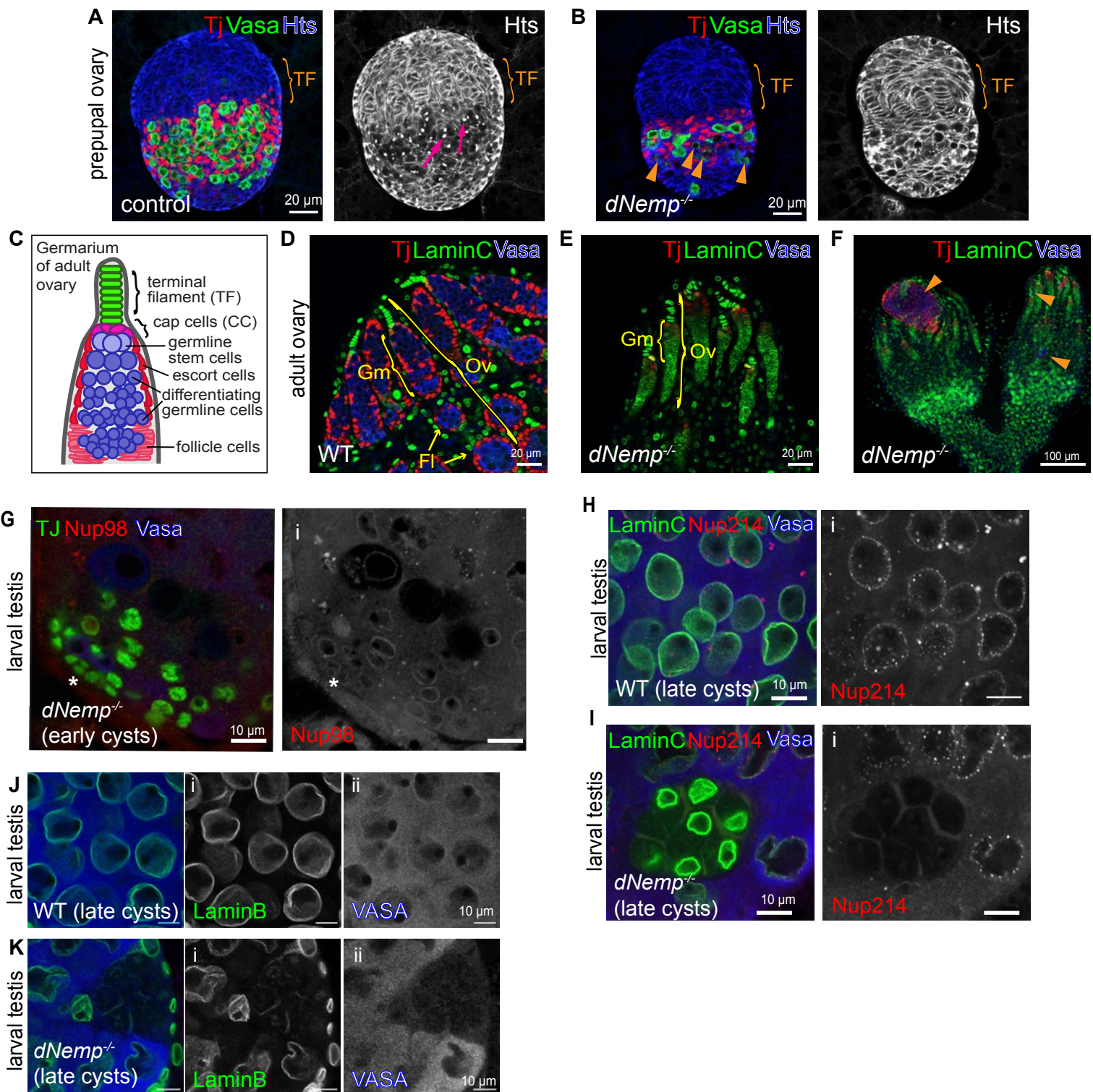


fig. S5. Characterization of gonadal defects in *dNemp* mutants. (A-B) The number of germline cells is strongly reduced in the *dNemp^{-/-}* ovary compared to control. WT (A) and *dNemp^{-/-}* (B) ovaries stained with Vasa, Tj, and Huli-tai-shao (Hts) which marks spectrosomes/fusomes (pink arrows), an organelle of germline cells. Arrowheads point to disintegrating Vasa staining, indicative of germline cell death. (C) Schematic of adult gerarium showing germline cells (blue) and surrounding somatic cell types. Ovaries from WT (D) and *dNemp^{-/-}* mutants (E-F), showing loss of germ cells in the adult. Ovaries are stained for Tj, a marker for somatic cells contacting germline cells, the germline marker Vasa and LaminC. Germline cells are either missing (E) or reduced to very few remaining ones (F, arrow heads) in *dNemp^{-/-}* mutant ovaries. Ov, ovariole, Gm, germarium, Fl, follicle. (G) Larval testis stained for nuclear pore protein, Nup98 (i), along with Tj and VASA in *dNemp* mutant testes. Asterisk marks the hub. The NE of early cyst cells appear intact, while occasional later cysts lack Nup98. (H-I) Nup214 (i), along with Vasa and LaminC in (H) WT and (I) *dNemp^{-/-}* testes show lack of Nup and increase of LaminC staining in late stage cysts. (J-K) LaminB (i) and Vasa (ii) staining of (J) WT and (F) *dNemp^{-/-}* larval testes.

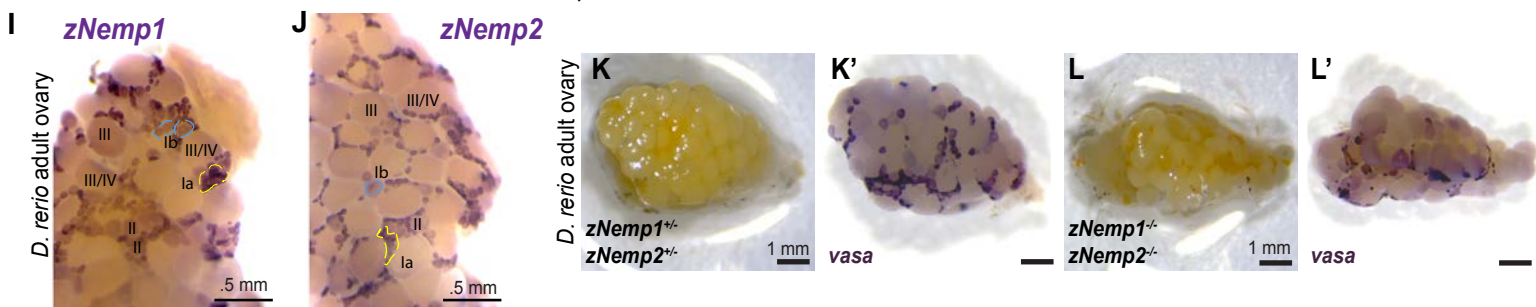
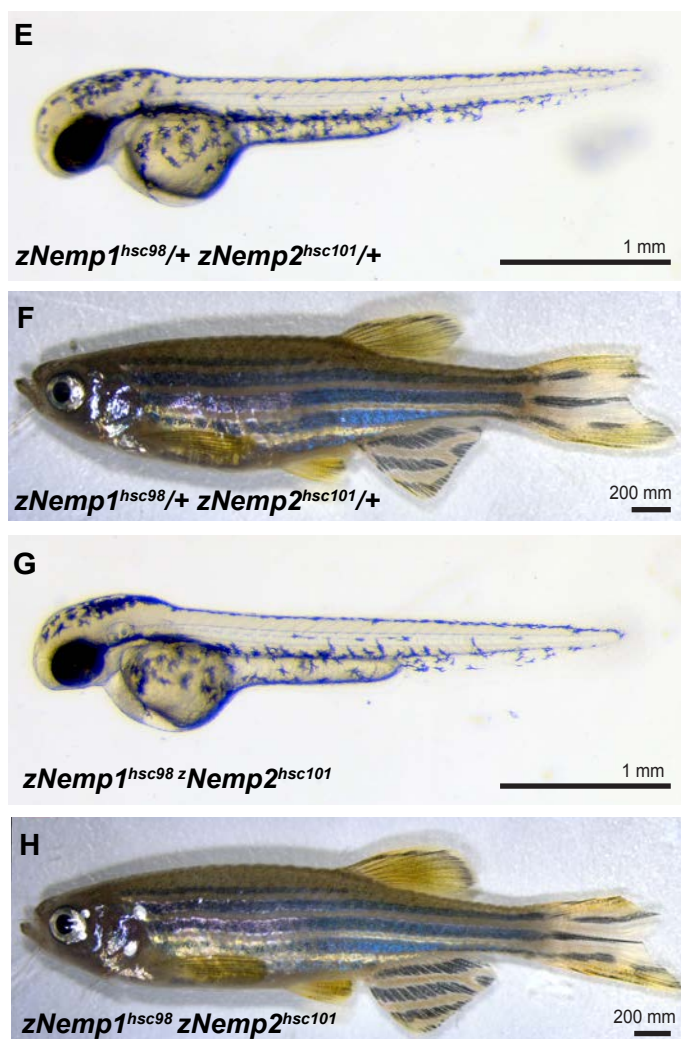
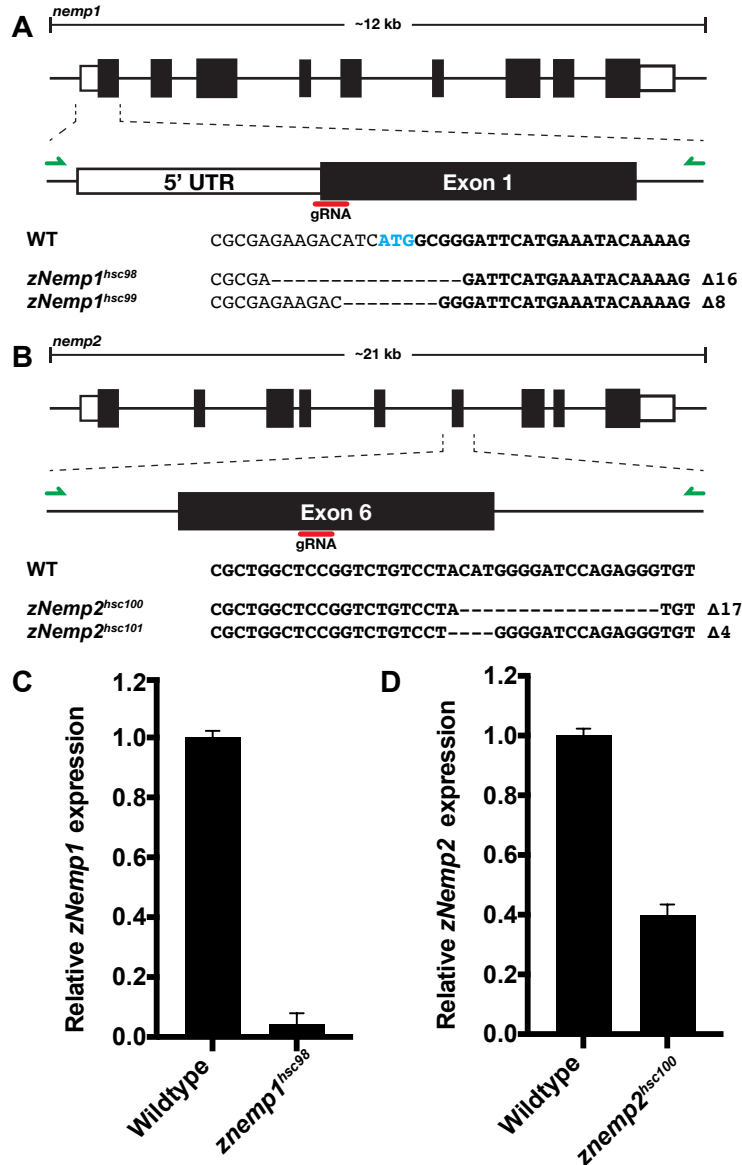


fig. S6. Generation and characterization of Zebrafish *Nemp* mutants. CRISPR targeting strategy to generate loss-of-function alleles of (A) *zNemp1* and (B) *zNemp2*. Quantitative RT-PCR of (C) *zNemp1* in *zNemp1hsc98* mutants and of (D) *zNemp2* in *zNemp2hsc100* mutants showing the reduction in transcript compared to wildtype. (E-H) *zNemp1hsc98*; *zNemp2hsc100* double homozygous mutants do not display any overt embryonic (E, G) or adult (F, H) phenotypes compared to *zNemp1hsc98/+*; *zNemp2hsc100/+* double heterozygous siblings. Photo Credit: Curtis Boswell, University of Toronto. (I-J) Whole mount RNA *in situ* hybridization of ovaries probed against *D. rerio* (I) *zNemp1* and (J) *zNemp2* shows predominant expression within stage Ia and Ib oocytes. (K-L') Lateral images of freshly-dissected (K-L) and Vasa-probed (K'-L') ovaries from *zNemp1hsc98*; *zNemp2hsc100* double mutants compared to *zNemp1hsc98/+*; *zNemp2hsc100/+* double heterozygous siblings showing a severe reduction in *Vasa*+ signal.

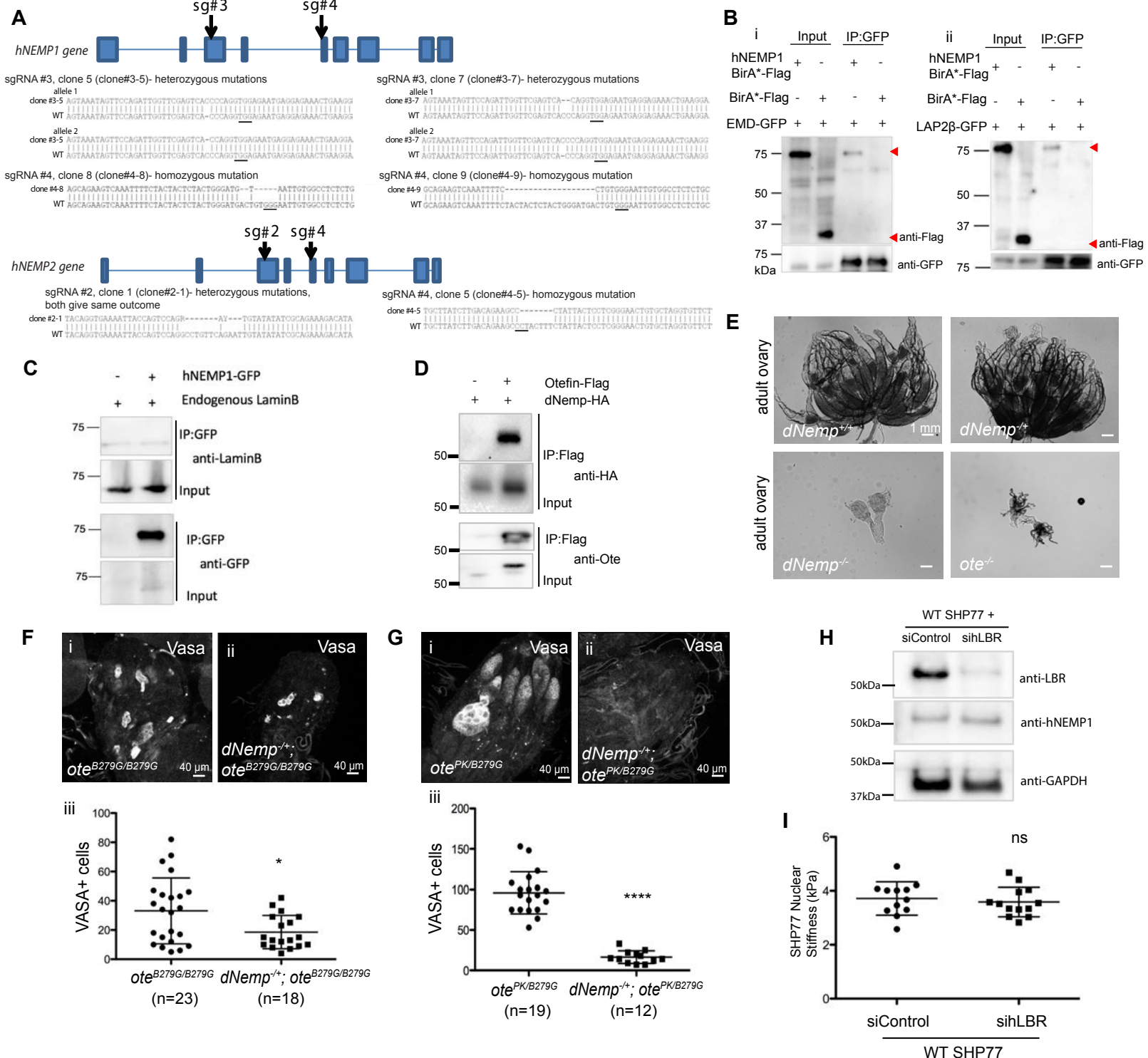


fig. S7. Nemp interacts with Emerin. (A) *hNEMP1* and -2 gene organization with arrows pointing to respective sgRNAs targets. Alignment of *hNEMP1* and -2 knockout clones compared to WT counterparts. The PAM sequence for the sgRNA is underlined in the WT sequence. *hNEMP1* clones #3-5 and #3-7 each contain different mutations in each allele, both are shown. *hNEMP1* + 2 clone #2-1 contains 2 different mutations, but each result in a similar 10bp deletion. (B) HEK293 cells stably expressing either *hNEMP1*-BirA*-Flag or BirA*-Flag and transfected with EMD-GFP (i), LAP2 β -GFP (ii) and subjected to GFP pull down followed by western blot using antibodies against Flag (top) or GFP (bottom). (C) HEK293 cells transiently transfected with or without *hNEMP1*-GFP and subjected to GFP pull down followed by western blot using antibodies against endogenous LaminB (top) or GFP (bottom). (D) *Drosophila* Kc cells transiently transfected with HA-tagged dNemp either alone or with Flag-tagged Otefin (Ote) were subjected to Flag pulldown followed by western blot against antibodies to HA (top) or Ote (bottom). dNemp and Ote form a complex. (E) Phase contrast images of *dNemp*^{+/+}, *dNemp*^{-/-}, *dNemp*^{-/-} and *ote*^{-/-} (*ote*^{B279G/B279G}) adult ovaries. (F-G) Vasa germ cell marker in the germarial regions of (i) *ote*^{-/-} (*ote*^{B279G/B279G} in (F) and *ote*^{PK/B279G} in (G)) and (ii) *dNemp*^{+/+}; *ote*^{-/-} adult ovaries. (iii) Quantification of Vasa+ cells from *ote*^{-/-} and *dNemp*^{+/+}; *ote*^{-/-} ovaries. Note loss of Vasa+ cells in *ote*^{-/-} mutants lacking a single copy of *dNemp*. (H-I) Immunoblot of SHP77 cells treated with siControl and sihLBR show a marked decrease in LBR protein in (H). GAPDH used as loading control. Apparent Young's Modulus of SHP77 cell nuclei treated with siControl and sihLBR in (I).

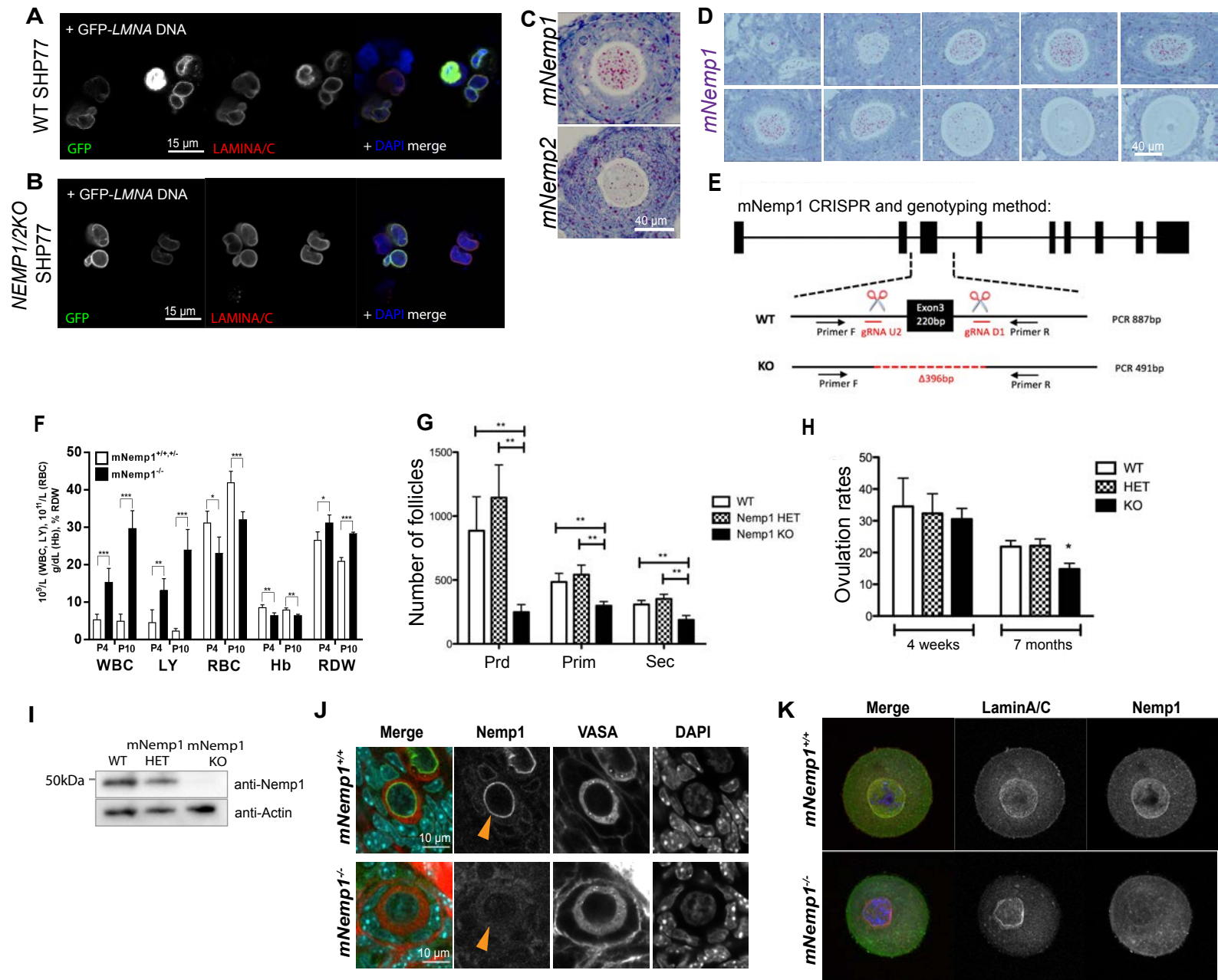


fig. S8. Generation and analysis of *mNemp1* mutant mice. (A-B) Immunofluorescence of WT (A) and *NEMP1/2KO* (B) SHP77 cells transfected with GFP-LMNA. (C) In situ hybridization of secondary follicles in WT mouse ovaries with *mNemp1* (top) or *mNemp2* (bottom) probes. (D) RNAscope in situ hybridization of P21 WT mouse ovary with a *mNemp1* probe showing high levels of *mNemp1* transcripts that progressively decrease with oocyte development (upper left: primordial oocyte, lower right: antral oocyte). (E) CRISPR strategy and genotyping method used to generate *mNemp1*^{-/-} mice. (F) Comparative blood analysis of *mNemp1*^{-/-} and *mNemp1*^{+/+, +/−} showing elevated counts of white blood cells (WBC) and lymphocytes (LY), and lower counts of red blood cells (RBC) accompanied by lower levels of hemoglobin (Hb) and increased distribution width (RDW) that reflects the size distribution spread of red blood cells (n=3 KO, 6 HET and WT (P4), n=4 KO, 5 HET and WT (P10)). (G) Follicle counts from 7 month-old ovaries (n=6 WT, 5 HET and 8 KO). (H) Ovulation rates across *mNemp1* genotypes at 4 weeks and 7 months (n=4 WT, 3 HET, 3 KO (4 weeks); n=7 WT, 6 HET, 13 KO (7 months)). (I) *mNemp1* immunoblotting of *mNemp1*^{+/+} (WT), *mNemp1*^{+/-} (HET) and *mNemp1*^{-/-} (KO) mouse ovary lysates. (J) Immunostaining of ovaries showing NE localization of *mNemp1* in primordial oocytes labeled with VASA. *mNemp1* NE staining disappears in *mNemp1*^{-/-} primordial oocytes. Orange arrowheads mark the NE. (K) Immunostaining of germinal vesicles from *mNemp1*^{+/+} and *mNemp1*^{-/-} mice. *mNemp1* NE staining disappears in KO oocytes.

Table S1: BioID results for hNEMP1-BirA*-Flag as bait with HEK lysate.

Prey Accession	PreyGene	Spectra	Spec Sum	Avg Spec	ctrlCounts	AvgP	MaxP	Fold	BFDR
4507555	LAP2β	152 215	367	183.5	17 14 34 26 51 16 16 19 26 22 54 31 18 34	1	1	5.02	0
14149680	ESYT1	140 145	285	142.5	7 9 4 10 16 5 9 14 11 7 16 10 5 12	1	1	11.21	0
4557553	EMD	117 128	245	122.5	3 4 4 7 0 2 5 5 9 7 6 14 8 9	1	1	14.29	0
264681410	LEMD3	110 119	229	114.5	5 5 4 3 0 2 6 3 2 0 0 2 0 7	1	1	24.29	0
4557303	ALDH3A2	84 80	164	82	4 4 4 3 6 0 3 5 9 4 3 7 2 5	1	1	14.35	0
115270970	CLCC1	64 94	158	79	2 0 0 5 3 2 0 0 0 0 0 0 0 0 0	1	1	46.08	0
170763517	TACC1	68 83	151	75.5	4 4 7 5 10 3 3 4 3 0 3 0 4 0	1	1	13.91	0
102467484	SMPD4	76 71	147	73.5	0 0 0 0 0 0 0 0 0 0 0 0 0 0 0	1	1	735	0
19923790	RAB3GAP2	64 78	142	71	4 0 4 0 0 0 0 2 0 0 0 0 3 2	1	1	33.13	0
4758012	CLTC	59 76	135	67.5	19 24 18 15 3 5 14 11 0 0 0 0 0 0	1	1	4.46	0
146260268	SMCR8	59 73	132	66	0 0 0 0 0 0 0 0 0 0 0 0 0 0 0	1	1	660	0
148664230	ANKLE2	60 68	128	64	0 0 0 0 0 2 0 3 0 0 0 2 0 2 0	1	1	49.78	0
27477136	ZC3HAV1	61 67	128	64	7 4 15 11 24 5 7 11 12 13 17 13 9 12	1	1	4.23	0
24430149	NUP155	62 56	118	59	4 7 0 10 0 0 2 3 3 0 0 0 0 0 0	1	1	14.24	0
21070997	STIM1	45 72	117	58.5	0 0 0 4 0 0 0 0 0 0 0 0 0 0 0	1	1	102.38	0
124378039	SEC16A	59 57	116	58	5 2 2 3 0 5 0 2 0 2 0 0 0 0 0	1	1	19.33	0
223029424	LSG1	51 65	116	58	8 5 0 3 9 0 4 2 5 7 3 9 7 4	1	1	8.12	0
118498356	KTN1	56 55	111	55.5	6 0 0 0 0 5 0 0 0 0 0 0 0 0 0	1	1	35.32	0
18079218	OSBPL8	50 56	106	53	6 7 0 10 4 2 6 7 6 0 0 5 0 5	1	1	7.89	0
94721250	VAPA	46 58	104	52	3 2 3 3 3 4 3 0 8 0 5 4 6 6	1	1	10.11	0
223555917	MTDH	51 53	104	52	15 8 14 8 19 14 17 9 2 5 13 3 6 4	1	1	3.6	0
5032093	SLC1A5	69 33	102	51	5 4 6 11 6 0 7 8 4 3 7 2 7 4	1	1	6.87	0
31542661	TMEM57	52 41	93	46.5	0 0 0 0 0 0 0 0 0 0 0 0 0 0 0	1	1	465	0
155030244	VEZT	66 26	92	46	0 0 0 0 0 0 0 0 0 0 0 0 0 0 0	1	1	460	0
171906582	CCDC47	44 44	88	44	0 0 0 0 6 0 3 0 4 0 0 0 0 5	1	1	17.11	0
17986258	MYL6	23 65	88	44	13 7 8 6 7 7 5 7 2 2 0 0 2 0	0.98	1	5.6	0
23308697	SRPR	41 46	87	43.5	5 0 0 0 0 0 0 3 0 0 2 0 5	1	1	20.3	0
38679909	TEX2	42 44	86	43	0 0 0 0 0 0 0 0 0 0 0 0 0 0 0	1	1	430	0
289547212	RAB3GAP1	31 55	86	43	0 0 0 0 0 0 3 0 0 2 0 2 0 0 0	1	1	43	0
29789403	PDZD8	36 48	84	42	0 0 0 0 0 0 2 0 0 0 0 0 0 0 0	1	1	147	0
389886539	TOR1AIP1	41 40	81	40.5	0 0 0 0 0 2 0 2 0 0 0 3 3 4	1	1	20.25	0
19920317	CKAP4	34 47	81	40.5	13 5 0 11 5 13 10 7 2 0 0 0 2 3	1	1	4.43	0
93277076	CDKAL1	40 40	80	40	0 0 0 0 0 0 0 0 0 0 0 0 0 0 0	1	1	400	0
194440707	VRK2	36 44	80	40	0 0 0 0 0 0 0 0 0 0 0 0 0 0 0	1	1	400	0
122891870	MIA3	38 40	78	39	0 0 0 0 0 0 0 0 0 0 0 0 0 0 0	1	1	390	0
5031877	LMNB1	35 43	78	39	12 7 0 7 7 6 8 3 0 0 0 3 3 0	1	1	5.46	0
4506289	PTPN1	38 39	77	38.5	3 2 0 0 0 3 4 0 4 3 2 4 2 4	1	1	10.78	0
5730120	YKT6	39 38	77	38.5	2 0 0 2 2 0 5 3 12 8 6 10 6 0	1	1	5.39	0
45387945	ESYT2	37 39	76	38	3 0 0 0 0 0 2 3 0 0 0 0 0 3 0	1	1	24.18	0
22749415	STT3A	59 17	76	38	4 6 0 4 5 0 5 6 3 0 0 0 0 3	1	1	8.06	0

Table S2: Flag-IP AP-MS results for hNEMP1-BirA*-Flag as bait with HEK lysate.

Prey Accession	PreyGene	Spectra	SpecSum	AvgSpec	ctrlCounts	AvgP	MaxP	SaintScore	Fold	BFDR
NP_001737.1	CANX	101 96	197	98.5	5 15 19 16	1	1	1	7.16	0
NP_733765.1	ATP2A2	58 55	113	56.5	0 6 3 9	1	1	1	12.56	0
NP_006316.1	RAN	39 36	75	37.5	2 4 1 7	1	1	1	10.71	0
NP_000692.2	ATP1A1	33 28	61	30.5	0 14 2 9	0.96	0.97	0.96	4.88	0.01
NP_000108.1	EMD	34 24	58	29	0 9 0 0	0.99	1	0.99	12.89	0
NP_001124147.1	CLGN	34 14	48	24	0 0 0 0	1	1	1	240	0
NP_938148.1	GANAB	22 25	47	23.5	0 6 0 6	0.99	0.99	0.99	7.83	0
NP_005906.2	MCM6	21 25	46	23	0 5 5 3	1	1	1	7.08	0
NP_079152.3	ADCK4	23 21	44	22	0 2 0 0	1	1	1	44	0
NP_008869.1	SNRPD1	20 22	42	21	0 6 2 4	1	1	1	7	0
NP_057479.2	PTPLAD1	14 18	32	16	0 1 2 3	1	1	1	10.67	0
NP_001106849.1	FANCI	13 18	31	15.5	0 0 1 0	1	1	1	62	0
NP_006109.2	HAX1	17 12	29	14.5	0 0 0 6	0.97	0.98	0.97	9.67	0.01
NP_004732.2	NOLC1	12 17	29	14.5	0 4 1 5	0.98	1	0.98	5.8	0.01
NP_060481.3	ARGLU1	17 11	28	14	4 6 1 0	0.93	0.99	0.93	5.09	0.01
NP_004362.2	COPA	10 16	26	13	0 0 2 5	0.96	0.99	0.96	7.43	0.01
NP_877577.1	MCM7	5 21	26	13	0 0 3 0	0.95	1	0.95	17.33	0.01
NP_612510.1	TECR	14 12	26	13	0 4 0 0	0.99	0.99	0.99	13	0
NP_061895.3	TMX3	15 11	26	13	0 5 1 0	0.97	0.99	0.97	8.67	0.01
NP_002379.3	MCM3	7 18	25	12.5	0 0 2 3	0.97	1	0.97	10	0.01
NP_005262.1	GLUD1	10 14	24	12	0 0 0 7	0.94	0.96	0.94	6.86	0.01
NP_001531.1	HSPB1	13 11	24	12	0 0 0 0	1	1	1	120	0
NP_005397.1	ROCK1	5 18	23	11.5	0 0 2 0	0.98	1	0.98	23	0
NP_006787.2	AFG3L2	11 9	20	10	0 0 0 0	1	1	1	100	0
NP_002941.1	RPN1	7 12	19	9.5	0 0 0 0	1	1	1	95	0
NP_036419.3	ACAP2	6 8	14	7	0 2 0 0	0.99	1	0.99	14	0
NP_065779.1	ESYT2	9 4	13	6.5	0 0 0 0	1	1	1	65	0
NP_068803.1	HIST1H4J	7 6	13	6.5	0 0 0 0	1	1	1	65	0
NP_001018146.1	NME1-NME2	8 5	13	6.5	0 0 2 0	0.98	1	0.98	13	0.01
NP_002873.1	RANBP1	6 7	13	6.5	0 0 0 0	1	1	1	65	0
NP_001020.2	RPS26	9 4	13	6.5	0 2 1 0	0.95	1	0.95	8.67	0.01
NP_001021.1	RPS27	5 8	13	6.5	0 0 0 0	1	1	1	65	0
NP_680090.1	CTSB	8 4	12	6	0 0 0 0	1	1	1	60	0
NP_001002762.2	DNAJB12	7 5	12	6	0 1 0 2	0.98	1	0.98	8	0
NP_003396.1	YWHAH	6 6	12	6	0 0 0 3	0.94	0.94	0.94	8	0.01
NP_001168.1	ARL1	6 5	11	5.5	0 2 0 0	0.97	0.98	0.97	11	0.01
NP_001035937.1	ABHD12	6 4	10	5	0 0 0 0	1	1	1	50	0
NP_079095.3	DCAKD	5 5	10	5	0 0 0 0	1	1	1	50	0
NP_006302.2	NCOR1	5 5	10	5	0 0 0 2	0.96	0.96	0.96	10	0.01
NP_001129243.1	RPN2	4 6	10	5	0 0 0 2	0.95	0.98	0.95	10	0.01

NP_008854.2	SDF2	5 5	10	5 0 0 0 0	1	1	1	50	0
NP_055472.1	TTI1	6 4	10	5 0 0 0 0	1	1	1	50	0
NP_919415.2	VAPA	6 4	10	5 0 0 0 0	1	1	1	50	0
NP_004729.1	VAPB	4 6	10	5 0 0 0 0	1	1	1	50	0
NP_066390.1	HIST1H2AE	5 4	9	4.5 2 0 0 0	0.94	0.96	0.94	9	0.01
NP_112092.1	APOL2	4 4	8	4 0 0 0 0	1	1	1	40	0
NP_001015048.1	BAG5	4 4	8	4 0 0 0 0	1	1	1	40	0
NP_006081.1	CEPT1	4 4	8	4 0 0 0 0	1	1	1	40	0
NP_001041675.1	CLCC1	6 2	8	4 0 0 0 0	0.99	1	0.99	40	0
NP_004636.1	COIL	4 4	8	4 0 0 0 0	1	1	1	40	0
NP_112601.3	CPVL	2 6	8	4 0 0 0 0	0.99	1	0.99	40	0
NP_055577.1	DHCR24	5 3	8	4 0 0 0 0	1	1	1	40	0
NP_003850.1	DPM1	4 4	8	4 0 0 0 0	1	1	1	40	0
NP_001120729.1	SLC39A10	6 2	8	4 0 0 0 0	0.99	1	0.99	40	0
NP_036451.3	SLC39A6	3 5	8	4 0 0 0 0	1	1	1	40	0
NP_001099000.1	CAP1	4 3	7	3.5 0 0 0 0	1	1	1	35	0
NP_004453.3	FDFT1	3 4	7	3.5 0 0 0 0	1	1	1	35	0
NP_000131.2	FECH	2 5	7	3.5 0 0 0 0	0.99	1	0.99	35	0
NP_783859.1	PTPMT1	4 3	7	3.5 0 0 0 0	1	1	1	35	0
NP_001252518.1	RTN3	4 3	7	3.5 0 0 0 0	1	1	1	35	0
NP_620116.1	BAX	3 3	6	3 0 0 0 0	1	1	1	30	0
NP_001127891.1	CDC7	3 3	6	3 0 0 0 0	1	1	1	30	0
NP_060886.1	FOXJ2	2 4	6	3 0 0 0 0	0.99	1	0.99	30	0
NP_002056.2	GLUL	2 4	6	3 0 0 0 0	0.99	1	0.99	30	0
NP_004209.2	RAB11B	4 2	6	3 0 0 0 0	0.99	1	0.99	30	0
NP_056174.2	SLC39A14	4 2	6	3 0 0 0 0	0.99	1	0.99	30	0
NP_055839.3	XPO7	4 2	6	3 0 0 0 0	0.99	1	0.99	30	0
NP_110438.1	MRPS26	3 2	5	2.5 0 0 0 0	0.98	1	0.98	25	0
NP_036614.1	ZNF281	2 3	5	2.5 0 0 0 0	0.98	1	0.98	25	0
NP_001153218.1	ABR	2 2	4	2 0 0 0 0	0.97	0.97	0.97	20	0.01
NP_689956.2	BRAT1	2 2	4	2 0 0 0 0	0.97	0.97	0.97	20	0.01
NP_689474.1	C12orf23	2 2	4	2 0 0 0 0	0.97	0.97	0.97	20	0.01
NP_115788.1	CYSTM1	2 2	4	2 0 0 0 0	0.97	0.97	0.97	20	0.01
NP_710154.1	IKBIP	2 2	4	2 0 0 0 0	0.97	0.97	0.97	20	0.01
NP_004765.2	MED1	2 2	4	2 0 0 0 0	0.97	0.97	0.97	20	0.01
NP_002860.2	RAB6A	2 2	4	2 0 0 0 0	0.97	0.97	0.97	20	0.01
NP_001139526.1	SNCA	2 2	4	2 0 0 0 0	0.97	0.97	0.97	20	0.01

SUPPLEMENTAL MATERIALS AND METHODS

CONTACT FOR REAGENT AND RESOURCE SHARING

Further information and requests for resources and reagents should be directed to and will be fulfilled by the Lead Contact, Helen McNeill (mneillh@wustl.edu) via applicable Lunenfeld-Tanenbaum Research Institute or Washington University Material Transfer Agreements and/or licensing agreements through the Office of Technology Management at the Lunenfeld-Tanenbaum Research Institute or Washington University School of Medicine.

EXPERIMENTAL MODEL AND SUBJECT DETAILS

Mice

All mouse experiments performed in Toronto, Canada were done so in accordance with the Canadian Council on Animal Care (CCAC) guidelines for Use of Animals in Research and Laboratory Animal Care under protocol AUP#20-0006H approved by animal care committee at The Toronto Centre for Phenogenomics. Mice were maintained on standard chow with 12h on/off light/dark cycle.

Mouse experiments performed in St. Louis, US were housed at the Mouse Genetic Core barrier facility (Dr. M. Wallace) located at the East McDonnell Building at the Washington University School of Medicine. Animal protocols used in this project strictly adhere to the ethical and sensitive care and use of animals in research and were approved by the Washington University School of Medicine Animal Studies Committee (Animal Welfare Assurance Permit # A-3381-01, Protocol# 20180186). *mNemp1^{-/-}* mice were generated in the C57BL/6N background (see below for details).

METHOD DETAILS

Immunostaining - larval wings

Larval wings were treated as larval testes, but placed in 70% glycerol before mounting.

Immunostaining – adult and larval ovaries

Adult and larval ovaries were dissected in PBS, fixed in 5% paraformaldehyde for 12-15 minutes, washed with PBT (PBS + 0.3% Triton X-100), blocked with PBTBS (PBT with 5% goat serum and 0.2% bovine serum albumin), incubated with primary antibody in PBTBS at 4°C overnight, washed with PBT, blocked with PBTBS , incubated in secondary antibody in PBT for 2 hours, washed with PBT, incubated in a 1:1 mix of PBT and Vectashield overnight at 4°C, and mounted in fresh Vectashield. Imaging was done with a 40x/1.4 Plan-Apo objective, using a Leica TCS SP8 confocal laser scanning microscope (Leica Microsystems). Images represent either individual optical sections or projections or Z-stacks (1 μm intervals) as indicated.

EdU Click-iT reaction

EdU incorporation into DNA was detected using the Click-iT™ EdU Alexa Fluor® Imaging kit (Invitrogen). All steps of the Click-iT™ reaction were performed at room temperature. Pre-pupal

testes were dissected and incubated into S2 culture media containing FBS with 20 µM EdU for 10 minutes. Testes were washed in 0.1% PBT and fixed in 4%PFA for 30 min. EdU cocktail containing Alexa Fluor 488 was added for 30 minutes followed by incubation with antibodies as per immunostaining protocol.

Transmission Electron Microscopy

Testis samples for transmitted electron microscopy (TEM) were prepared as previously described (27). Briefly, Drosophila third instar larval or adult testes were dissected in cold 0.1 M sodium PB (phosphate buffer), pH 7.4. Samples were fixed in cold Trumps fixative (4% paraformaldehyde, 1% glutaraldehyde, 0.005% CaCl₂ in PB) for 1 hour, at 4°C, and post fixed in 1% OsO₄ for 1 hour. After thorough rinsing, samples were subjected to an ethanol-dehydration series (30%, 70%, 90%, 100% ethanol), followed by a 2 X 10min incubation with propylene oxide. Dehydrated samples were incubated overnight in 1:1 propylene oxide:resin mix. Samples were embedded in Quetol-Spurr resin. Ultrathin sections were viewed with a JEOL JTE141011 TEM (JEOL, Peabody, MA; The Hospital for Sick Children Electron Microscopy Facility). Images were obtained using AmtV542 acquisition software. Micrographs were uniformly adjusted for brightness and contrast using Adobe Photoshop.

Generating a *dNemp* null allele

Two mutants (*dNemp*^{RR1} and ^{RR2}) were generated using homologous ends out recombination as described previously (28). Homologous flanking regions of the *dNemp* locus were cloned into pRK2 using primers DHRF1 and DHRR1 for the downstream homologous region primers UHRF1 and UHRR1 for the upstream homologous region (Primer Table). The complete targeting construct was injected into flies by BestGene Inc. with standard P-element protocol. Transgenes on the 3rd chromosome were then crossed to the BDSC#6935-hid line expressing Flipase and SceI endonuclease. Progeny was heat shocked in a 37°C water bath for 90 min. Successful excision resulted in majority white eyed flies. Flies were crossed to balancer stocks and progeny was screened for recombinant flies by the presence of red eyes. Red-eyed males were selected and crossed to X chromosome balancer stock virgins.

Molecular confirmation of *dNemp* null allele

Flies were tested with PCR for absence of the coding region of *dNemp* and the correct placement of the *white* gene replacing the *dNemp* codons. Single fly PCR was performed on candidate nulls as described in Supplemental fig. S3A with primers described in the Primer Table below.

Generation of transgenic flies carrying rescue constructs

BAC constructs for rescue experiments were obtained using BAC clones ch322118I15, CH322-12P09 and CH322-158k07 (BAC PAC resource Centre, Oakland Research Institute). DNA was prepped by BestGene Inc. and injected into flies at the attP2 site on 3L using PhiC31 standard protocol. Rescue experiments using BAC lines were performed by crossing *dNemp*/FM7 females to BAC/TM6 males.

Selecting *dNemp* mutants for larval testes dissection

dNemp null flies were generated as described above (see **Generating a *dNemp* null allele**). For selection of *dNemp* mutants, *dNemp* null/*FM7-GFP* flies were placed in cages and allowed to lay eggs on grape plates for 4-8 hours. 24 hours later, larvae were selected and placed on new plates to be aged until late 3rd instar. Mutant males were selected based on absence of GFP.

Generating *dNemp* mutant females

Females from a *dNemp*/*FM7-GFP* balanced stock were crossed to males that had the *dNemp* mutation on the X and a BAC rescue transgene on the 3rd chromosome balanced over TM6. These male flies are fertile, as the BAC rescues fertility. Female progeny without *FM7* and with TM6 were homozygous *dNemp* null mutants with no BAC rescue construct.

Generating flies bearing a *dNemp*-FRT chromosome generating mutant clones

dNemp mutants balanced over *FM7* were crossed to *FRT19A* males. *dNemp*/*FRT19A* females were then crossed to *FM7* balancer stock males. Recombinants were selected by presence of red eyes, marking the *dNemp* allele, and ability to live on G418 food, marking the FRT site.

Generation of targeted lesions of *zNemp1* and *zNemp2*

Targeted lesions within the coding sequences of zebrafish *nemp1* (*zNemp1*) and *nemp2* (*zNemp2*) were generated by CRISPR/Cas9 mutagenesis (29). Briefly, *zNemp1* and *zNemp2* guide RNA target sequences were synthesized into overlapping oligonucleotides and cloned into pT7-gRNA. Plasmid templates were linearized with BamHI, *in vitro* transcribed using the MEGAshortscript T7 kit (Thermo Fisher Scientific) and cleaned up by ammonium acetate precipitation. Cas9 mRNA was prepared using the pT3TS-nCas9n plasmid and the mMessage mMachine T3 kit (Thermo Fisher Scientific). An injection mix containing 50 pg of guide RNA and 150 pg of Cas9 mRNA were co-injected into wildtype 1-cell embryos and raised to adulthood. Offspring generated from these F0 fish were screened by PCR using primers listed in Primer Table for loss of either FauI (*zNemp1*) or BamHI (*zNemp2*) and genomic lesions were confirmed by Sanger sequencing. Heterozygous F1 animals for *zNemp1*^{hsc98} and *zNemp2*^{hsc100} were maintained separately and intercrossed to generate viable F2 homozygous offspring. Homozygous *zNemp1*^{hsc98} and *zNemp2*^{hsc100} animals were intercrossed to produce double heterozygous animals, which were then bred for viable double knockout mutants.

Molecular Cloning of *zNemp1* and *zNemp2*

The coding sequences of *zNemp1* and *zNemp2* were amplified from 24 hpf cDNA libraries generated from wildtype embryos following primers listed in Primer Table: *nemp1* ME F, *nemp1* ME R, *nemp2* ME F, *nemp2* ME R. Fragments were gel extracted, cloned into pDONR221 via Gateway recombination (Invitrogen) and sequence verified. Clones were further shuttled into pCS2+ for probe synthesis.

Ovary *in situ* hybridization in Zebrafish

Digoxigenin-labelled *vasa* probe was generated by XbaI endonuclease digestion of a pBluescript SK(-)-based vector followed by *in vitro* transcription with T7 RNA polymerase (DIG RNA Labeling Kit, Roche). Probes for *zNemp1* and *zNemp2* were generated from clones described above by NotI digestion followed by *in vitro* transcription with T7 RNA polymerase. Probes were purified by lithium chloride precipitation, resuspended in RNase-free water and diluted to a working concentration of 1 ng/µL in hybridization buffer. *In situ* hybridization on adult gonads was performed as described (30, 31).

qRT-PCR

qRT-PCR was performed using 10 ng of total RNA in a one-step qRT-PCR reaction (Luna Universal One-Step RT-qPCR Kit, New England Biolabs) and performed on a Roche Lightcycler 96 system. Primers were designed to span exons to prevent genomic amplification, and are listed in Primer Table. Ct values were obtained for each gene and normalized to *efla*. Fold change was calculated relative to wildtype expression according to the equation $2^{-\Delta\Delta C_t}$. Standard error was calculated as standard deviation of the fold change according to the equation: $\text{stdevfoldchange} = (\ln 2)(\text{stdev}^{\Delta\Delta C_t})(2^{-\Delta\Delta C_t})$, where $\text{stdev}^{\Delta\Delta C_t} = \sqrt{(\text{stdev of reference})^2 + (\text{stdev of gene of interest})^2}$. All graphs are representative of two independent experiments with three technical replicates.

Generating cell lines for BirA mass spectrometry

Human *NEMP1* (*hNEMP1*) was cloned through gateway cloning first into pDON221 using the Gateway BP reaction, and then into the V8449 pDEST pcDNA5 – BirA*-Flag-C-terminal vector. HEK293 Flp-In T-Rex cells (Thermo Fisher Scientific) were transfected with this hNemp1-BirA*-FLAG construct along with the FLP recombinase construct p0G44 using Effectene Reagent (Qiagen). Stable cell lines were generated through hygromycin selection. Individual clones of stable cells were grown up and maintained individually.

Human cell transfections

For experiments with combined hNemp1 and hNemp2 knockdown, the indicated cells were transfected with 40 nM control, non-targeting siRNA (siControl) or 20 nM each hNemp1 or hNemp2 ON-TARGETplus siRNA (Dharmacon) using Dharmafect 1 transfection reagent as per manufacturer's instructions. Three days following siRNA transfection, cells were transfected a second time and cell numbers counted 3 days later.

Proteomics - BioID

HEK293 cells expressing hNemp1-BirA*-Flag or BirA*-Flag alone cell pellets from two 70-80% confluent 150mm plates were lysed in RIPA buffer at a 1:10 pellet weight:volume ratio. RIPA buffer was 50 mM Tris-HCl pH 7.5, 150 mM NaCl, 1% Triton X-100, 1mM EDTA, 1 mM EGTA, 0.1%SDS, Sigma protease inhibitors P8340 at 1:500, and 0.5% Sodium deoxycholate. After addition of RIPA buffer to the frozen cell pellet, 1ul of benzonase (250U) was added to each sample and the pellets resuspended by incubating at 4°C with agitation for 20 minutes. Once resuspended, samples

were sonicated (3 x 10 second bursts with 2 seconds rest in between) on ice at 65% amplitude using a Qsonica with a CL-18 probe. Sonicated lysates were centrifuged for 30 min at 20,817 x g and supernatants transferred to 15mL falcon tubes with a 30uL bed volume of washed streptavidin-sepharose beads (GE Cat# 17-5113-01). Affinity purification was performed at 4°C on a nutator for 3 hours, and then the beads pelleted (400 x g, 1 min), the supernatant removed, and the beads transferred to a 1.5mL tube in 1 mL RIPA buffer (minus protease inhibitors and sodium deoxycholate). The beads were washed by pipetting with an additional 1mL RIPA buffer (minus protease inhibitors and sodium deoxycholate) followed by two washes in TAP lysis buffer (50mM HEPES-KOH pH 8.0, 100mM KCl, 10% glycerol, 2mM EDTA, 0.1% NP-40), and 3 washes in 50mM ammonium bicarbonate pH 8 (ABC). After the last wash proteins digested on bead in 30uL of 50mM ABC pH 8 including 1 ug trypsin at 37°C overnight with mixing. After digestion an additional 0.5 ug of trypsin was added to each sample (in 10uL 50mM ABC) and the samples incubated an additional 2 hours at 37°C. Beads were rinsed and these rinses combined with the original supernatant. Pooled supernatant was acidified to 2% formic acid. Dried samples were resuspended in 12 uL 5% formic acid, 6 uL taken for analysis by mass spectrometry (5 uL injected by autosampler).

Proteomics – Flag AP-MS

HEK293 cells expressing hNemp1-BirA*-Flag or BirA*-Flag alone from two 70-80% confluent 150mm plates were lysed by passive lysis assisted by freeze-thaw. Lysis buffer was 50 mM Hepes-KOH pH 8.0, 100 mM KCl, 2 mM EDTA, 0.1% NP40, 10% glycerol, 1 mM PMSF, 1 mM DTT and Sigma protease inhibitor cocktail, P8340, 1:500. Frozen/thawed sample lysates were transferred to 15 ml conical tubes containing a 12.5uL bed volume of washed anti-FLAG M2 magnetic beads (SIGMA M8823). Affinity purification was performed at 4°C on a nutator for 2 hours. Beads were washed and samples were trypsin digested, resuspended in formic acid to a final concentration of 2%. Dried samples were resuspended in 12uL 5% formic acid, and 6uL taken for analysis by mass spectrometry (5uL injected by autosampler).

Mass spectrometric analysis

Samples were analyzed by reversed phase liquid chromatography coupled to mass spectrometry on an Velos Orbitrap or a Velos Orbitrap Elite (Thermo Scientific) mass spectrometer equipped with a nano-spray ion source (Proxeon Biosystems). The HPLC program delivered an acetonitrile gradient over 145min and the data were acquired in CID mode (centroid) in a data-dependent manner with MS/MS on the 10 most abundant parent ions (isolated species were put on an exclusion list for 30s). RAW mass spectrometry files were converted to mzXML using ProteoWizard (3.0.4468) and analyzed using the iProphet pipeline implemented within ProHits as follows (32). The database consisted of the human and adenovirus complements of the RefSeq protein database (version 57) supplemented with “common contaminants” from the Max Planck Institute (<https://maxquant.org/maxquant/>) and the Global Proteome Machine (GPM; <http://www.thegpm.org/crap/index.html>). The search database consisted of forward and reversed sequences (labeled “DECOY”); in total 72226 entries were searched. The search engines used were Mascot (2.3.02; Matrix Science) and Comet (2012.01 rev.3; with trypsin specificity (2 missed

cleavages were allowed) and deamidation (NQ) and oxidation (M) as variable modifications. The parent mass tolerance was set at 12–15 ppm while the fragment bin tolerance was set at 0.6 amu. The resulting Comet and Mascot search results were individually processed by PeptideProphet, and peptides were assembled into proteins using parsimony rules first described in ProteinProphet into a final iProphet protein output using the Trans-Proteomic Pipeline (TPP; Linux version, v0.0 Development trunk rev 0, Build 201303061711). TPP options were as follows: general options are -p0.05 -x20 -PPM -d"DECOY", iProphet options are -ipPRIME and PeptideProphet options are -OpdP. All proteins with a minimal iProphet protein probability of 0.05 were parsed to the relational module of ProHits. Note that for analysis with SAINT, only proteins with iProphet protein probability ≥ 0.95 are considered and 2 unique peptides are considered. This corresponds to an estimated protein-level FDR of $\sim 0.5\%$.

Interaction scoring

The results were analyzed by SAINTexpress (v 3.3 for the AP-MS dataset; v 3.6.1 for the BioID dataset) (33). The controls were “compressed” to increase the stringency of the filtering (compression to n takes the n highest values for each detected prey across all the controls and use those for SAINT modeling) (34). For the FLAG data, 4 negative controls were compressed to 2 while the 14 controls for BioID (consisting BirA*-FLAG alone or cells not expressing BirA*) were compressed to 7. SAINT probabilities computed independently for each bait replicate are averaged, and the average probability (AvgP) is reported as the final SAINT score used to calculate the Bayesian FDR. Preys with BFDR <1% were considered “true” interactors. All mass spectrometry data was deposited to ProteomeXchange through partner MassIVE (massive.ucsd.edu) and given the following identifiers: PXD012913 and MSV00083498 (AP-MS dataset) and PXD012912 and MSV000083497 (BioID dataset).

Generating SHP77 knockout cell clones

The LentiCRISPR v2 vector (Addgene Plasmid, 52961) was used to generate knockout cells using hNemp1 sgRNA #3; hNemp1sgRNA #4; hNemp2 sgRNA #2 and hNemp2 sgRNA #4 (see Key Resource Table below for sequences). Following viral transduction, SHP77 cells were selected in puromycin (4 μ g/ml), then single cell clones generated by limiting dilution. Targeting was confirmed by sequencing genomic DNA. Two clones from a control, non-targeting sgRNA (clones #2 and #5), 2 clones from the hNemp1 sgRNA #3 (clones #3-5 and #3-7) and 2 clones from the hNemp1 sgRNA #4 (clones #4-8 and #4-9) were generated. For the combined hNemp-1 and 2 knockout, the original sghNemp1 clone #3-7 was transduced with sequences targeting hNemp2. One clone from hNemp2 sgRNA #2 (clone A#3-7 + B#2-1) and 1 clone from the hNemp2 sgRNA #4 (clone #3-7 + B#4-5) were further characterized.

In Situ hybridization of mouse ovaries

ISH was performed on ovary sections with the RNAscope 2.0 Red Kit (Advanced Cell Diagnostics). Whole ovaries dissected from 4 weeks-old C57BL6/N mice were fixed in 4% PFA/PBS overnight at

4°C and embeded in paraffin. Five μ m-thick microtome sections were deparaffinized in xylene, followed by dehydration in an ethanol series. Upon antigen retrieval, sections were rinsed with water and immediately treated with protease. Hybridization with custom-made *mNemp1* (targeting 1031-2117 of NM_001113211.1) and *mNemp2* (targeting 957-1999 of NM_001142647.1) RNAscope probes, preamplifier and amplifier were carried out at 40°C followed by development using the Fast Red reagents. Control hybridizations were carried out in parallel with all test hybridizations. Samples were counterstained with Hematoxylin and imaged with a DS-Fi2 color camera mounted on a Ti2 microscope (Nikon).

Apoptosis by flow cytometry

RPE-1 apoptosis was assayed using Annexin V and PI staining as per manufacturer's protocol (BD Biosciences). Cells were analyzed using a Gallios flow cytometer (Beckman Coulter) and data analyzed using Kaluza or ModFit software.

Analysis of mouse peripheral blood

Whole blood was collected by venipuncture of the facial vein and immediately transferred in blood collection tubes (BD Microtainer). Blood samples were mixed and placed under the Hemavet HV950 probe (Drew Scientific, Inc.) for analysis using reagents from the LV-PAK (Drew Scientific Inc.). Multi-Trol mouse serum controls (Drew Scientific, Inc.) were used for calibration of the Hemavet HV950. Collected blood was also spread on glass slides for Wright-Giemsa staining according to the manufacturer's protocol (Wright-Giemsa Stain Modified, Sigma-Aldrich).

Immunocytochemistry

Oocytes fixed in PHEM fixative were blocked in 10% horse serum in PBS and stained using anti-acetylated tubulin antibody (1:1000; Key Resource Table) or stained with anti-mouse Nemp1 generated as described above. After overnight incubation and washes, secondary antibody used was anti mouse or anti rabbit Alexa 488 (Bethyl) and cells were stained with DAPI solution. Oocytes were then scored for spindle presentation using Axioplan microscope (Zeiss).

Micropipette aspiration of germinal vesicles

Germinal vesicle oocytes were collected by puncturing large antral follicles ~46h after gonadotropin priming (5IU PMSG, Folligon, Merck). Cumulus cells were manually stripped by pipetting. Cumulus cells free oocytes from either WT and Nemp1 KO females were subsequently used for assessment of nuclear membrane stiffness.

The micropipette aspiration system consists of an inverted microscope (Nikon Eclipse TS100) with a motorized XY translation stage (ProScan, Prior Scientific Inc.), two micromanipulators (MX7600, Siskiyou, Yreka, CA) mounted with a micropipette. In experiments, a holding micropipette was connected to a pneumatic pump (PX409-10WDWU5V, Omega Engineering, Stamford, CT) to immobilize the oocyte within the field of view, and another micropipette with an inner diameter of 5 μ m was mounted on the micromanipulator and connected to an oil pump (CellTram Vario, Eppendorf

Canada Ltd.) which is controlled by a stepper motor (Phidgets Inc.). The oocyte was placed in the mHTF medium (LifeGlobal, Guilford, USA) supplemented with 0.1% HSA and 1 μ M milrinone (Sigma Aldrich, Oakville, Canada) in petri dish, and immobilized by the holding micropipette though applying a negative pressure by the pneumatic pump. The aspiration pipette was positioned close to the oocyte as described in (35) and was used to penetrate into the oocyte and reach the nuclear envelope. The camera (Basler scA1300-32gm) recorded the nuclear envelope deformation while a negative pressure was applied by the aspiration pipette with the oil pump.

Through recording the deformation caused by the applied negative pressure, the mechanical properties of the oocyte nucleus were calculated through the following relationship,

$$D(t) = \frac{\varphi a \Delta P}{\pi k_1} \left(1 - \frac{k_2}{k_1 + k_2} e^{\frac{t}{\tau}} \right)$$

where $D(t)$ represents the recorded nuclear envelope deformation, ΔP is the pressure applied, φ is the wall function related to the ratio of the micropipette wall thickness to the pipette radius, a is the radius of the nucleus, τ is the time constant for the exponential term, k_1 and k_2 are elastic constant within the viscoelastic model, and the equilibrium Young's modulus was calculated as, $E = \frac{3}{2} k_1$ (36). The data processing was performed in an off-line manner using MATLAB, with the code available through https://github.com/XianShawn/oocyte_nucleus.

Genetic analysis in the UK Biobank study

We analysed genetic data from the March 2018 “v3” release of UK Biobank, a resource extensively described elsewhere [<https://doi.org/10.1101/166298>]. Age at natural menopause was defined using the same criteria as the ReproGen consortium (37), yielding a sample size of 106,353 women with genotype and phenotype. In addition to the quality control metrics performed centrally by UK Biobank, we defined a subset of “white European” ancestry samples using a K-means clustering approach applied to the first four principle components calculated from genome-wide SNP genotypes (38). Individuals clustered into this group who self-identified by questionnaire as being of an ancestry other than white European were excluded. Association testing was performed using a linear mixed models implemented in BOLT-LMM (39) to account for cryptic population structure and relatedness. Only autosomal genetic variants which were common ($MAF > 1\%$), passed QC in all 106 batches and were present on both genotyping arrays were included in the genetic relationship matrix (GRM). Genotyping chip and age at baseline were included as binary covariates. Association testing at the *hNEMPI* gene locus was assessed using two significance thresholds. Firstly, we considered only genome-wide significant variants ($P < 5 \times 10^{-8}$) within 500kb of *NEMPI*. Secondly, we assessed any protein truncating variants detected in the GTEx project (5) and corrected for the number of variants tested ($N=1$, $P < 0.05$).

QUANTIFICATION AND STATISTICAL ANALYSES

Statistical comparison of *Drosophila* fertility, proliferation rates, germ cell counts, *C. elegans* brood size and Zebrafish fertility were performed using Student’s paired t-test. *Drosophila* germ cell

circularity ratio and *C. elegans* sterility were compared using Student's un-paired t-test. *Drosophila* eclosure rates were compared using one-way analysis of variance (ANOVA). Statistical analysis of differences for all cell line experiments was determined by a Mann-Whitney Rank Sum Test. AFM and micropipette aspiration analysis were statistically compared using Student's paired t-test or one-way ANOVA.

Statistical comparison for murine breeding data, follicle counts and ovulation rates were performed using one-way ANOVA. Chromosomal misalignment and significance of interaction between age and genotype was confirmed by two-way analysis of variance using Sigma Stat statistical package (Systat). Embryo progression was calculated via the Kaplan-Meier method using the Prism GraphPad program. The log-rank (Mantel-Cox) test was used to statistically confirm the difference in progression between the various genotypes.

*: $0.05 > P > 0.01$; **: $0.01 > P > 0.001$; ***: $0.001 > P > 0.0001$; ****: $P < 0.0001$. All means are expressed +/- SEM. N indicates experimental replicates, n indicates the number of data points. More specialized statistical analyses are detailed in the main text and figure legends.

PRIMER TABLE

Primer name	Sequence (5'-3')	Purpose
<i>Zebrafish</i>		
Zenemp1 Geno F	AGACGCGCGGTTCCCTCTG	Genotyping <i>nemp1</i> alleles
Zenemp1 Geno R	TTCAATGATGGGACGGCTGG	Genotyping <i>nemp1</i> alleles
Zenemp2 Geno F	TGAAAGACCTGTAATGGGTGTG	Genotyping <i>nemp2</i> alleles
Zenemp2 Geno R	GACTGTTACTACGCAATGCTGG	Genotyping <i>nemp2</i> alleles
Zenemp1 ME F	GGGGACAAGTTGTACAAAAAAGCAGGCTTCGCCACCATGGCGGGATTATGAAATAC	Cloning full-length zebrafish <i>nemp1</i>
Zenemp1 ME R	GGGGACCACCTTGACAGAAAGCTGGGTATTATTCGGCTGTGTTGTT	Cloning full-length zebrafish <i>nemp1</i>
Zenemp2 ME F	GGGGACAAGTTGTACAAAAAAGCAGGCTTCGCCACCATGGAGAAACTGGCTGCTT	Cloning full-length zebrafish <i>nemp2</i>
Zenemp2 ME R	GGGGACCACCTTGACAGAAAGCTGGGTATTCAAAAGAAGCTGGCTGGTCTTC	Cloning full-length zebrafish <i>nemp2</i>
Zenemp1 qRT F	TTCGCGAACAGACCAATGAGA	qRT-PCR primer for <i>nemp1</i>
Zenemp1 qRT R	AGCAACACTCCAGGCCAGAAAA	qRT-PCR primer for <i>nemp1</i>
Zenemp2 qRT F	TTCGTGTGCTGGCTGATACTG	qRT-PCR primer for <i>nemp2</i>
Zenemp2 qRT R	GCGTGAGGAAGACAAATGTGG	qRT-PCR primer for <i>nemp2</i>
eif1a F	TGGGCACCTGCTCGTTGA	Housekeeping gene for qRT-PCR
eif1a R	TACCCCTCCTTGCGCTCAATC	Housekeeping gene for qRT-PCR
<i>Drosophila</i>		
dNemp FR1	CATCAAGCATAAGCAAGTCAGC	screening of dNemp allele (region 1)
dNemp RR1	ATGCCGACCAAGATAGTAGAAC	screening of dNemp allele (region 1)
dNem FR2	CGACCATGTGCTGGCTATC	screening of dNemp allele (region 2)
dNemp RR2	GAACGAGGCAGCGCAAAG	screening of dNemp allele (region 2)
dNemp F1	GCCTTGGTTGAATCGGAATC	screening of <i>white</i> recombination
dNemp R1	CGACTTCGCCACCGATAACGGAC	screening of <i>white</i> recombination
white FW1	GCCTTGGTTGAATCGGAATC	screening of <i>white</i> downstream junction
white RW1	CGAGGGTCTGCTGATTAACC	screening of <i>white</i> upstream junction
CTLF1	GACGATCCAGCGGCATATCC	PCR amplification control
CTLR1	CCTACGGAATGAATCAGCACG	PCR amplification control
DHRF1	AAAAAGATCTGCTGACTGCTTATGCTTGATG	Cloning of dNemp downstream homologous region
DHRR1	AAAACCTAGCGTCACCGAGTTCTGATATCTG	Cloning of dNemp downstream homologous region
UHRF1	AAAAGCGGCCCTCGAACTCCACAACGAATAGC	Cloning of dNemp upstream homologous region
UHRR1	AAAACATATGGACCACC ACGTTCTATGCTGTA	Cloning of dNemp upstream homologous region
<i>Mouse</i>		
mGenoF1	ACTGATCCTTGCTTGTATGATCTC	mNemp1 ^{-/-} mice forward genotyping primer
mGenoR1	ACTGTTAGCTTCCTGTCTCAA	mNemp1 ^{-/-} mice reverse genotyping primer

KEY RESOURCES TABLE

REAGENT or RESOURCE	SOURCE	IDENTIFIER
Antibodies		
mouse anti-Arm, 1:400	DSHB	Cat# N27A1-c
rat anti-E-cad, 1:400	DSHB	Cat# DCAD2-c
mouse anti-LamDm0, 1:1000	DSHB	Cat#ADL67.10-c
mouse anti-LamC, 1:500	DSHB	Cat#LC28.26-c
mouse anti-Eyes absent, 1:100	DSHB	Cat#eya10H6-c
mouse anti-Bam, 1:50	DSHB	Cat#bam-s
mouse anti-Notch, 1:500	DSHB	Cat#C17.9C6
mouse anti-gp210, 1:50	DSHB	Cat#AGP26.10
mouse anti Hts: 1:5	DSHB	Cat#1B1
guinea pig anti-Tj, 1:5000	Dr. Dorothea Godt	Clone G5/G6
rabbit anti-Zfh-1, 1:400	Dr. Ruth Lehmann	N/A
rabbit anti-STAT, 1:1,000	Dr. Erika Bach	N/A
rabbit anto-Chinmo, 1:1000	Dr. Erika Bach	N/A
rabbit anti-eIF4E-3, 1:800	Dr. Paul Lasko	N/A
rabbit anti-RanGap, 1:50	Dr. Julia Zeitlinger	N/A
chicken anti-Vasa, 1:500	Dr. Ken Howard	N/A
rabbit anti-Vasa, 1:3000	Dr. Ruth Lehmann and Dr. Paul Lasko	N/A
goat anti-Otefin, 1:1000	Dr. Pamela Geyer	N/A
rabbit anti-Boule 1:1000	Dr. Steven Wasserman	N/A
rabbit anti-Nup214, 1:1000	Dr. Yiqun Yao	N/A
rabbit anti-p-smad3, 1:500	Cell Signaling Technology	Cat#9520
rabbit anti-pMad1/5, 1:100	Cell Signaling Technology	Cat#9516
rabbit anti-GFP, 1:500	Abcam	Cat#ab290
mouse M2 anti-Flag, 1:1000	Sigma-Aldrich	Cat#F1804
rat anti-HA, 1:1000	Sigma-Aldrich	Cat#11867423001
rabbit anti-Vasa, 1:500	Santa Cruz Biotechnology	Cat#sc-30210
rat anti-dNemp, 1:500	This paper	N/A
goat anti-VASA, 1:500	Santa Cruz Biotechnology	Cat#sc-26877
rabbit anti-mNemp1, 1:600	This paper	N/A
mouse anti-Actin, 1:1000	Millipore	Cat#MAB1501
rabbit anti-EMD	Sigma	Cat#HPA000609
goat anti-LaminB1 1:1000	Santa Cruz Biotechnology	Cat#sc-6216
mouse anti-LaminB receptor (LBR) 1:1000	Abcam	Cat#ab232731
mouse anti-LaminA/C 1:1000	Millipre	Cat#SAB4200236
mouse anti-VASA 1:500	Abcam	Cat#ab27591
PE-conjugated anti-Ter119	Biolegend	Cat#116208
APC-conjugated anti-CD71	eBioscience	Cat#17-0711-82
CD16/32	Biolegend	Cat#101302
FITC-conjugated Annexin-V with propidium iodide	Biolegend	Cat#640914

rabbit anti-Emerin	Santa Cruz Biotechnology	Cat#15378
mouse anti-acetylated tubulin antibody	Sigma-Aldrich	Cat#T7451
Biological Samples		
Multi-Trol mouse serum controls	Drew Scientific, Inc.	Cat#600070
mHTF medium	Life Global	Cat# LGFR-100
human chorionic gonadotropin	Merck	Cat#230734
pregnant mare's serum gonadotropin (PMSG)	Prospec	Cat#HOR-272
Latrunculin B	Sigma	Cat#428020
Chemicals, Peptides, and Recombinant Proteins		
Rhodamine-phalloidin	Invitrogen	Cat#R415
Lysotracker DND-99	Invitrogen	Cat#L7528
Effectene transfection reagent	Qiagen	Cat#301427
Critical Commercial Assays		
Click-iT™ EdU Alexa Fluor® Imaging kit	Invitrogen	Cat#C10337
Streptavidin-coupled Dynabeads	Thermo Fisher Scientific	Cat#11205D
GFP-Trap_A	Chromotek GmbH	Cat#gtak-20
anti-Flag M2 affinity gel	Sigma-Aldrich	Cat#A2220
Anti-HA agarose	Sigma-Aldrich	Cat#A2095
mMessage mMachine T3 kit (Thermo Fisher)	Thermo Fisher Scientific	Cat# AM1348
MEGAshortscript T7 kit	Thermo Fisher Scientific	Cat#AM1354
DIG RNA Labeling Kit	Roche	Cat#11277073910
LV-PAK	Drew Scientific Inc.	Cat#200108
RNAscope 2.0 Red Kit	Advanced Cell Diagnostics	Cat#322350
Wright-Giemsa Stain, Modified	Sigma-Aldrich	Cat#WG32-1L
Luna Universal One-Step RT-qPCR Kit	New England Biolab	Cat#E3005
Experimental Models: Cell Lines		
S2 cells	DGRC	Stock#6
HEK293	ATCC	Cat#CRL-1573, RRID:CVCL_0045
SHP77	ATCC	Cat#CRL-2195, RRID:CVCL_1693
T24	ATCC	Cat# HTB-4, RRID:CVCL_0554
NCI-H661	ATCC	Cat# HTB-183, RRID:CVCL_1577
hTERT-RPE-1	ATCC	Cat# CRL-4000, RRID:CVCL_4388
HEK293 Flp-In T-Rex cells	Thermo Fisher Scientific	R78007
Experimental Models: Organisms/Strains		
<i>D.melanogaster</i> : y[1] w[*] N[1]/FM7c, P{w[+mC]=GAL4-tw.i.G}108.4, P{UAS-2xEGFP}AX	Bloomington Drosophila Stock Center	RRID:BDSC_6873
<i>D.melanogaster</i> : nanos Gal4-VP16 w[*]; pBac{w[+mW.hs]=GreenEye.nosGal4}DmeI6	Bloomington Drosophila Stock Center	RRID:BDSC_32180
<i>D.melanogaster</i> : alphaTub84B Gal4 y[1]w[*]; P{w[+mc]=tubP-Gal4}LL7/Tm3, Sb[1]Ser[1]	Bloomington Drosophila Stock Center	RRID:BDSC_5138
<i>D.melanogaster</i> : y[*] w[*]; P{w[+mW.hs]=GawB}NP1624 / CyO, P{w[-]}=UAS-lacZ.UW14}UW14	Kyoto Stock Center	

<i>D.melanogaster</i> : dNemp rescue w[1118]; P{UASp-dNemp-HA}	This paper	
<i>D.melanogaster</i> : hNEMP1 rescue w[1118]; P{UASp-hNEMP1-HA}	This paper	
<i>D.melanogaster</i> : y[1] w[1118] P{ry[+t7.2]=neoFRT}19A	Bloomington Drosophila Stock Center	RRID:BDSC_1744
<i>D.melanogaster</i> : y[1] w[67c23]; P{y[+t7.7]=CaryP}attP2	Bloomington Drosophila Stock Center	RRID:BDSC_8622
<i>D.melanogaster</i> : RNAi of dNemp1: w ¹¹⁸ ; P{TRiP.HMC04788}attP40	VDRC	Cat#37412
<i>D.melanogaster</i> : RNAi of dNemp1 for germ cell knockdown y[1] sc[*] v[1]:P{y[+t7.7]v[+t1.8]=TRiP.HMC04788}attP40	Bloomington Drosophila Stock Center	RRID:BDSC_57475
<i>D.melanogaster</i> : <i>dNemp1</i> null allele	This paper	N/A
<i>D.melanogaster</i> : y[1] w[1118]; P{ry[+t7.2]=70FLP}23 P{v[+t1.8]=70I-SceI}4A/TM3, Sb[1] Ser[1]	Bloomington Drosophila Stock Center	RRID:BDSC_6935
<i>D.melanogaster</i> : oteB279 w[1118]; pBac{w[+mc]=5HPw[+] }Ote[B279]/CyO, P{ry[+t7.2]=sevRas1.V12}FK1	Bloomington Drosophila Stock Center	RRID:BDSC_16189
<i>D.melanogaster</i> : otePK	P. Geyer; (12)	
<i>C.elegans</i> : <i>nemp-1(oz535)/sC1(s2023) [dpy-1(s2170) umnIs41] III</i>	<i>Caenorhabditis</i> Genetics Center, University of Minnesota	Cat#BS7012
<i>C.elegans</i> : <i>nemp-1(oz534)/sC1(s2023) [dpy-1(s2170) umnIs41] III</i>	<i>Caenorhabditis</i> Genetics Center, University of Minnesota	Cat#BS7011
ZeNemp1 ^{hsc98} , ZeNemp1 ^{hsc99} , ZeNemp2 ^{hsc100} and ZeNemp2 ^{hsc101}	This paper	
Mouse: mNemp1 null allele through deletion of exon3	This paper, Toronto Center for Phenogenomics	N/A
Mouse: mEMD null allele through deletion of exons2-6	(26)	
Oligonucleotides		
BAC clone ch322118I15	BAC PAC resource Centre, Oakland Research Institute	N/A
BAC clone CH322-12P09	BAC PAC resource Centre, Oakland Research Institute	N/A
BAC clone CH322-158k07	BAC PAC resource Centre, Oakland Research Institute	N/A
ZeNemp1 gRNA: 5'- GGAAACGCGAGAACATCA-3'		
ZeNemp2 gRNA: 5'-GGCTCCGGTCTGTCCTACAT-3'		
hNEMP1 ON-TARGETplus siRNA	Dharmacon	Cat#J-026966-19-005 and J-026966-21-005
hNEMP2 ON-TARGETplus siRNA	Dharmacon	Cat#L-186179-00-0005
hLBR ON-TARGETplus siRNA	Dharmacon	Cat#L-021505-00-0005
SHP77-hNemp1 sgRNA #3 ATTGGTTCGAGTCACCCAGG		
SHP77-hNemp1sgRNA #4 TACTCTACTGGGATGACTGT		

SHP77-hNemp2 sgRNA #2 TATACAATTCTAACAGGCC		
SHP77-hNemp2 sgRNA #4 CCCGAGGAGTAATAGAAAGT		
RNAscope mNemp1 ISH probe	ACD Bio	Cat#536641
RNAscope mNemp2 ISH probe	ACD Bio	Cat#536651
mNemp1 ^{-/-} mice gRNA_U2:	Toronto Center for Phenogenomics	N/A
mNemp1 ^{-/-} mice gRNA_D1:	Toronto Center for Phenogenomics	N/A
pDEST15 gateway vector	Thermo Fisher Scientific	Cat#11802014
pT7-gRNA	Wenboai Chen	Addgene plasmid # 46759
LentiCRISPR v2 vector	Feng Zhang	Addgene Plasmid# 52961
pT3TS-nCas9n	Wenboai Chen	Addgene plasmid # 46757
Recombinant DNA		
dNemp(301-454)-GST	This paper	N/A
hNemp1 (1-444)-BirA*-FLAG	This paper	N/A
BirA*-FLAG	This paper	N/A
dNemp-HA pPWH	This paper	N/A
dNEMP1-HA pPWH	This paper	N/A
hNEMP1-GFP pPWG	This paper	N/A
GFP-hLaminA	(40)	
Software and Algorithms		
EZ-CI 3.80	Nikon	N/A
NIS-Elements	Nikon	N/A
PRISM		N/A
Axiovision	Carl Zeiss	N/A
AmtV542	Advanced Microscopy Techniques	N/A
Other		
BD Microtainer	BD Biosciences	Cat#365974

REFERENCES AND NOTES

1. D. Goswami, G. S. Conway, Premature ovarian failure. *Hum. Reprod. Update* **11**, 391–410 (2005).
2. M. Horikoshi, F. R. Day, M. Akiyama, M. Hirata, Y. Kamatani, K. Matsuda, K. Ishigaki, M. Kanai, H. Wright, C. A. Toro, S. R. Ojeda, A. Lomniczi, M. Kubo, K. K. Ong, J. R. B. Perry, Elucidating the genetic architecture of reproductive ageing in the Japanese population. *Nat. Commun.* **9**, 1977 (2018).
3. L. Stolk, J. R. B. Perry, D. I. Chasman, C. He, M. Mangino, P. Sulem, M. Barbalic, L. Broer, E. M. Byrne, F. Ernst, T. Esko, N. Franceschini, D. F. Gudbjartsson, J.-J. Hottenga, P. Kraft, P. F. McArdle, E. Porcu, S.-Y. Shin, A. V. Smith, S. van Wingerden, G. Zhai, W. V. Zhuang, E. Albrecht, B. Z. Alizadeh, T. Aspelund, S. Bandinelli, L. B. Lauc, J. S. Beckmann, M. Boban, E. Boerwinkle, F. J. Broekmans, A. Burri, H. Campbell, S. J. Chanock, C. Chen, M. C. Cornelis, T. Corre, A. D. Coviello, P. d'Adamo, G. Davies, U. de Faire, E. J. C. de Geus, I. J. Deary, G. V. Z. Dedoussis, P. Deloukas, S. Ebrahim, G. Eiriksdottir, V. Emilsson, J. G. Eriksson, B. C. J. M. Fauser, L. Ferrelli, L. Ferrucci, K. Fischer, A. R. Folsom, M. E. Garcia, P. Gasparini, C. Gieger, N. Glazer, D. E. Grobbee, P. Hall, T. Haller, S. E. Hankinson, M. Hass, C. Hayward, A. C. Heath, A. Hofman, E. Ingelsson, A. C. J. W. Janssens, A. D. Johnson, D. Karasik, S. L. R. Kardia, J. Keyzer, D. P. Kiel, I. Kolcic, Z. Kutalik, J. Lahti, S. Lai, T. Laisk, J. S. E. Laven, D. A. Lawlor, J. Liu, L. M. Lopez, Y. V. Louwers, P. K. E. Magnusson, M. Marongiu, N. G. Martin, I. M. Klaric, C. Masciullo, B. M. Knight, S. E. Medland, D. Melzer, V. Mooser, P. Navarro, A. B. Newman, D. R. Nyholt, N. C. Onland-Moret, A. Palotie, G. Paré, A. N. Parker, N. L. Pedersen, P. H. M. Peeters, G. Pistis, A. S. Plump, O. Polasek, V. J. M. Pop, B. M. Psaty, K. Räikkönen, E. Rehnberg, J. I. Rotter, I. Rudan, C. Sala, A. Salumets, A. Scuteri, A. Singleton, J. A. Smith, H. Snieder, N. Soranzo, S. N. Stacey, J. M. Starr, M. G. Stathopoulou, K. Stirrups, R. P. Stolk, U. Styrkarsdottir, Y. V. Sun, A. Tenesa, B. Thorand, D. Toniolo, L. Tryggvadottir, K. Tsui, S. Ulivi, R. M. van Dam, Y. T. van der Schouw, C. H. van Gils, P. van Nierop, J. M. Vink, P. M. Visscher, M. Voorhuis, G. Waeber, H. Wallaschofski, H. E. Wichmann, E. Widen, C. J. M. Wijnands-van Gent, G. Willemsen, J. F. Wilson, B. H. R. Wolffenduttel, A. F. Wright, L. M. Yerges-Armstrong, T. Zemunik, L. Zgaga, M. C. Zillikens, M. Zygmunt; Life Lines Cohort Study, A. M. Arnold, D. I. Boomsma, J. E. Buring, L. Crisponi, E. W. Demerath, V. Gudnason, T. B. Harris, F. B. Hu, D. J. Hunter, L. J. Launer, A. Metspalu, G. W.

- Montgomery, B. A. Oostra, P. M. Ridker, S. Sanna, D. Schlessinger, T. D. Spector, K. Stefansson, E. A. Streeten, U. Thorsteinsdottir, M. Uda, A. G. Uitterlinden, C. M. van Duijn, H. Völzke, A. Murray, J. M. Murabito, J. A. Visser, K. L. Lunetta, Meta-analyses identify 13 loci associated with age at menopause and highlight DNA repair and immune pathways. *Nat. Genet.* **44**, 260–268 (2012).
4. C. Bycroft, C. Freeman, D. Petkova, G. Band, L. T. Elliott, K. Sharp, A. Motyer, D. Vukcevic, O. Delaneau, J. O'Connell, A. Cortes, S. Welsh, A. Young, M. Effingham, G. M. Vean, S. Leslie, N. Allen, P. Donnelly, J. Marchini, The UK Biobank resource with deep phenotyping and genomic data. *Nature* **562**, 203–209 (2018).
5. M. A. Rivas, M. Pirinen, D. F. Conrad, M. Lek, E. K. Tsang, K. J. Karczewski, J. B. Maller, K. R. Kukurba, D. S. De Luca, M. Fromer, P. G. Ferreira, K. S. Smith, R. Zhang, F. Zhao, E. Banks, R. Poplin, D. M. Ruderfer, S. M. Purcell, T. Tukiainen, E. V. Minikel, P. D. Stenson, D. N. Cooper, K. H. Huang, T. J. Sullivan, J. Nedzel; GTEx Consortium, G. Consortium, C. D. Bustamante, J. B. Li, M. J. Daly, R. Guigo, P. Donnelly, K. Ardlie, M. Sammeth, E. T. Dermitzakis, M. I. McCarthy, S. B. Montgomery, T. Lappalainen, D. G. MacArthur, Effect of predicted protein-truncating genetic variants on the human transcriptome. *Science* **348**, 666–669 (2015).
6. H. Mamada, N. Takahashi, M. Taira, Involvement of an inner nuclear membrane protein, Nemp1, in *Xenopus* neural development through an interaction with the chromatin protein BAF. *Dev. Biol.* **327**, 497–507 (2009).
7. G. S. Wilkie, N. Korfali, S. K. Swanson, P. Malik, V. Srzen, D. G. Batrakou, J. de las Heras, N. Zuleger, A. R. W. Kerr, L. Florens, E. C. Schirmer, Several novel nuclear envelope transmembrane proteins identified in skeletal muscle have cytoskeletal associations. *Mol. Cell. Proteomics* **10**, M110.003129 (2011).
8. J. Swift, I. L. Ivanovska, A. Buxboim, T. Harada, P.C. D. P. Dingal, J. Pinter, J. D. Pajerowski, K. R. Spinler, J.-W. Shin, M. Tewari, F. Rehfeldt, D. W. Speicher, D. E. Discher, Nuclear lamin-A scales with tissue stiffness and enhances matrix-directed differentiation. *Science* **341**, 1240104 (2013).

9. D. I. Kim, B. KC, W. Zhu, K. Motamedchaboki, V. Doye, K. J. Roux, Probing nuclear pore complex architecture with proximity-dependent biotinylation. *Proc. Natl. Acad. Sci. U.S.A.* **111**, E2453–E2461 (2014).
10. L. J. Barton, A. A. Soshnev, P. K. Geyer, Networking in the nucleus: A spotlight on LEM-domain proteins. *Curr. Opin. Cell Biol.* **34**, 1–8 (2015).
11. X. Jiang, L. Xia, D. Chen, Y. Yang, H. Huang, L. Yang, Q. Zhao, L. Shen, J. Wang, D. Chen, Otefin, a nuclear membrane protein, determines the fate of germline stem cells in *Drosophila* via interaction with Smad complexes. *Dev. Cell* **14**, 494–506 (2008).
12. L. J. Barton, B. S. Pinto, L. L. Wallrath, P. K. Geyer, The *Drosophila* nuclear lamina protein otefin is required for germline stem cell survival. *Dev. Cell* **25**, 645–654 (2013).
13. D. Pan, L. D. Estévez-Salmerón, S. L. Stroschein, X. Zhu, J. He, S. Zhou, K. Luo, The integral inner nuclear membrane protein MAN1 physically interacts with the R-Smad proteins to repress signaling by the transforming Growth Factor- β superfamily of cytokines. *J. Biol. Chem.* **280**, 15992–16001 (2005).
14. B. S. Pinto, S. R. Wilmington, E. E. L. Hornick, L. L. Wallrath, P. K. Geyer, Tissue-specific defects are caused by loss of the *Drosophila* MAN1 LEM domain protein. *Genetics* **180**, 133–145 (2008).
15. J. Lammerding, J. Hsiao, P. C. Schulze, S. Kozlov, C. L. Stewart, R. T. Lee, Abnormal nuclear shape and impaired mechanotransduction in emerin-deficient cells. *J. Cell Biol.* **170**, 781–791 (2005).
16. H. Liu, J. Wen, Y. Xiao, J. Liu, S. Hopyan, M. Radisic, C. A. Simmons, Y. Sun, *In Situ* mechanical characterization of the cell nucleus by atomic force microscopy. *ACS Nano* **8**, 3821–3828 (2014).
17. X. Wang, H. Liu, M. Zhu, C. Cao, Z. Xu, Y. Tsatskis, K. Lau, C. Kuok, T. Filletter, H. McNeill, C. A. Simmons, S. Hopyan, Y. Sun, Mechanical stability of the cell nucleus – roles played by the cytoskeleton in nuclear deformation and strain recovery. *J. Cell Sci.* **131**, jcs209627 (2018).

18. C. Guilluy, L. D. Osborne, L. Van Landeghem, L. Sharke, R. Superfine, R. Garcia-Mata, K. Burridge, Isolated nuclei adapt to force and reveal a mechanotransduction pathway in the nucleus. *Nat. Cell Biol.* **16**, 376–381 (2014).
19. T. J. Kirby, J. Lammerding, Emerging views of the nucleus as a cellular mechanosensor. *Nat. Cell Biol.* **20**, 373–381 (2018).
20. S. Jorge, S. Chang, J. J. Barzilai, P. Leppert, J. H. Segars, Mechanical signaling in reproductive tissues: Mechanisms and importance. *Reprod. Sci.* **21**, 1093–1107 (2014).
21. J. E. Hornick, F. E. Duncan, L. D. Shea, T. K. Woodruff, Isolated primate primordial follicles require a rigid physical environment to survive and grow *in vitro*. *Hum. Reprod.* **27**, 1801–1810 (2012).
22. T. K. Woodruff, L. D. Shea, A new hypothesis regarding ovarian follicle development: Ovarian rigidity as a regulator of selection and health. *J. Assist. Reprod. Genet.* **28**, 3–6 (2011).
23. J. Link, D. Jahn, M. Alsheimer, Structural and functional adaptations of the mammalian nuclear envelope to meet the meiotic requirements. *Nucleus* **6**, 93–101 (2015).
24. B. Burke, LINC complexes as regulators of meiosis. *Curr. Opin. Cell Biol.* **52**, 22–29 (2018).
25. J. Link, V. Jantsch, Meiotic chromosomes in motion: A perspective from *Mus musculus* and *Caenorhabditis elegans*. *Chromosoma* **128**, 317–330 (2019).
26. G. Melcon, S. Kozlov, D. A. Cutler, T. Sullivan, L. Hernandez, P. Zhao, S. Mitchell, G. Nader, M. Bakay, J. N. Rottman, E. P. Hoffman, C. L. Stewart, Loss of emerin at the nuclear envelope disrupts the Rb1/E2F and MyoD pathways during muscle regeneration. *Human Mol. Gen.* **15**, 637–651 (2006).
27. L. Fabian, H.-C Wei, J. Rollins, T. Noguchi, J. T. Blankenship, K. Bellamkonda, G. Polevoy, L. Gervais, A. Guichet, M. T. Fuller, J. A. Brill, Phosphatidylinositol 4,5-bisphosphate directs spermatid cell polarity and exocyst localization in *Drosophila*. *Mol. Biol. Cell* **21**, 1546–1555 (2010).

28. J. Huang, S. Wu, J. Barrera, K. Matthews, D. Pan, The Hippo signaling pathway coordinately regulates cell proliferation and apoptosis by inactivating Yorkie, the *Drosophila* Homolog of YAP. *Cell* **122**, 421–434 (2005).
29. L.-E. Jao, S. R. Wente, W. Chen, Efficient multiplex biallelic zebrafish genome editing using a CRISPR nuclease system. *Proc. Natl. Acad. Sci. U.S.A.* **110**, 13904–13909 (2013).
30. B. W. Draper, Identification of germ-line stem cells in Zebrafish. *Methods Mol. Biol.* **1463**, 103–113 (2017).
31. B. W. Draper, C. M. McCallum, C. B. Moens, *nanos1* is required to maintain oocyte production in adult zebrafish. *Dev. Biol.* **305**, 589–598 (2007).
32. G. Liu, J. D. R. Knight, J. P. Zhang, C.-C. Tsou, J. Wang, J.-P. Lambert, B. Larsen, M. Tyers, B. Raught, N. Bandeira, A. I. Nesvizhskii, H. Choi, A.-C. Gingras, Data independent acquisition analysis in ProHits 4.0. *J. Proteomics* **149**, 64–68 (2016).
33. G. Teo, G. Liu, J. Zhang, A. I. Nesvizhskii, A.-C. Gingras, H. Choi, SAINTexpress: Improvements and additional features in Significance Analysis of Interactome software. *J. Proteomics* **100**, 37–43 (2014).
34. D. Mellacheruva, Z. Wright, A. L. Couzens, J.-P. Lambert, N. A. St-Denis, T. Li, Y. V. Miteva, S. Hauri, M. E. Sardiu, T. Y. Low, V. A. Halim, R. D. Bagshaw, N. C. Hubner, A. Al-Hakim, A. Bouchard, D. Faubert, D. Fermin, W. H. Dunham, M. Goudreault, Z.-Y. Lin, B. G. Badillo, T. Pawson, D. Durocher, B. Coulombe, R. Aebersold, G. Superti-Furga, J. Colinge, A. J. R. Heck, H. Choi, M. Gstaiger, S. Mohammed, I. M. Cristea, K. L. Bennett, M. P. Washburn, B. Raught, R. M. Ewing, A.-C. Gingras, A. I. Nesvizhskii, The CRAPome: A contaminant repository for affinity purification-mass spectrometry data. *Nat. Methods* **10**, 730–736 (2013).
35. X. Wang, Z. Zhang, H. Tao, J. Liu, S. Hopyan, Y. Sun, Characterizing inner pressure and stiffness of trophoblast and inner cell mass of blastocysts. *Biophys. J.* **115**, 2443–2450 (2018).
36. S. C. W. Tan, W. X. Pan, G. Ma, N. Cai, K. W. Leong, K. Liao, Viscoelastic behaviour of human mesenchymal stem cells. *BMC Cell Biol.* **9**, 40 (2008).

37. F. R. Day, K. S. Ruth, D. J. Thompson, K. L. Lunetta, N. Pervjakova, D. I. Chasman, L. Stolk, H. K. Finucane, P. Sulem, B. Bulik-Sullivan, T. Esko, A. D. Johnson, C. E. Elks, N. Franceschini, C. He, E. Altmaier, J. A. Brody, L. L. Franke, J. E. Huffman, M. F. Keller, P. F. McArdle, T. Nutile, E. Porcu, A. Robino, L. M. Rose, U. M. Schick, J. A. Smith, A. Teumer, M. Traglia, D. Vuckovic, J. Yao, W. Zhao, E. Albrecht, N. Amin, T. Corre, J.-J. Hottenga, M. Mangino, A. V. Smith, T. Tanaka, G. Abecasis, I. L. Andrulis, H. Anton-Culver, A. C. Antoniou, V. Arndt, A. M. Arnold, C. Barbieri, M. W. Beckmann, A. Beeghly-Fadiel, J. Benitez, L. Bernstein, S. J. Bielinski, C. Blomqvist, E. Boerwinkle, N. V. Bogdanova, S. E. Bojesen, M. K. Bolla, A.-L. Borresen-Dale, T. S. Boutin, H. Brauch, H. Brenner, T. Brüning, B. Burwinkel, A. Campbell, H. Campbell, S. J. Chanock, J. R. Chapman, Y.-D. I. Chen, G. Chenevix-Trench, F. J. Couch, A. D. Covello, A. Cox, K. Czene, H. Darabi, I. De Vivo, E. W. Demerath, J. Dennis, P. Devilee, T. Dörk, I. Dos-Santos-Silva, A. M. Dunning, J. D. Eicher, P. A. Fasching, J. D. Faul, J. Figueroa, D. Flesch-Janys, I. Gandin, M. E. Garcia, M. García-Closas, G. G. Giles, G. G. Girotto, M. S. Goldberg, A. González-Neira, M. O. Goodarzi, M. L. Grove, D. F. Gudbjartsson, P. Guénel, X. Guo, C. A. Haiman, P. Hall, U. Hamann, B. E. Henderson, L. J. Hocking, A. Hofman, G. Homuth, M. J. Hooning, J. L. Hopper, F. B. Hu, J. Huang, K. Humphreys, D. J. Hunter, A. Jakubowska, S. E. Jones, M. Kabisch, D. Karasik, J. A. Knight, I. Kolcic, C. Kooperberg, V.-M. Kosma, J. Kriebel, V. Kristensen, D. Lambrechts, C. Langenberg, J. Li, X. Li, S. Lindström, Y. Liu, J. Luan, J. Lubinski, R. Mägi, A. Mannermaa, J. Manz, S. Margolin, J. Marten, N. G. Martin, C. Masciullo, A. Meindl, K. Michailidou, E. Mihailov, L. Milani, R. L. Milne, M. Müller-Nurasyid, M. Nalls, B. M. Neale, H. Nevanlinna, P. Neven, A. B. Newman, B. G. Nordestgaard, J. E. Olson, S. Padmanabhan, P. Peterlongo, U. Peters, A. Petersmann, J. Peto, P. D. P. Pharoah, N. N. Pirastu, A. Pirie, G. Pistis, O. Polasek, D. Porteous, B. M. Psaty, K. Pylkäs, P. Radice, L. J. Raffel, F. Rivadeneira, I. Rudan, A. Rudolph, D. Ruggiero, C. F. Sala, S. Sanna, E. J. Sawyer, D. Schlessinger, M. K. Schmidt, F. Schmidt, R. K. Schmutzler, M. J. Schoemaker, R. A. Scott, C. M. Seynaeve, J. Simard, R. Sorice, M. C. Southey, D. Stöckl, K. Strauch, A. Swerdlow, K. D. Taylor, U. Thorsteinsdottir, A. E. Toland, I. Tomlinson, T. Truong, L. Tryggvadottir, S. T. Turner, D. Vozzi, Q. Wang, M. Wellons, G. Willemsen, J. F. Wilson, R. Winqvist, B. B. H. R. Wolffenbuttel, A. F. Wright, D. Yannoukakos, T. Zemunik, W. Zheng, M. Zygmunt, S. Bergmann, D. I. Boomsma, J. E. Buring, L. Ferrucci, G. W. Montgomery, V. Gudnason, T. D. Spector, C. M. van Duijn, B. Z. Alizadeh, M. Ciullo, L. Crisponi, D. F. Easton, P. P. Gasparini, C. Gieger, T. B. Harris, C. Hayward, S. L. R. Kardia, P. Kraft, B. M. Knight, A.

- Metspalu, A. C. Morrison, A. P. Reiner, P. M. Ridker, J. I. Rotter, D. Toniolo, A. G. Uitterlinden, S. Ulivi, H. Völzke, N. J. Wareham, D. R. Weir, L. M. Yerges-Armstrong; PRACTICAL consortium; kCon Fab Investigators; AOCS Investigators; Generation Scotland; EPIC-Inter Act Consortium; Life Lines Cohort Study; A. L. Price, K. Stefansson, J. A. Visser, K. K. Ong, J. Chang-Claude, J. M. Murabito, J. R. B. Perry, A. Murray, Large-scale genomic analyses link reproductive aging to hypothalamic signaling, breast cancer susceptibility and BRCA1-mediated DNA repair. *Nat. Genet.* **47**, 1294–1303 (2015).
38. F. R. Day, H. Helgason, D. I. Chasman, L. M. Rose, P.-R. Loh, R. A. Scott, A. Helgason, A. Kong, G. Masson, O. T. Magnusson, D. Gudbjartsson, U. Thorsteinsdottir, J. E. Buring, P. M. Ridker, P. Sulem, K. Stefansson, K. K. Ong, J. R. B. Perry, Physical and neuro-behavioural determinants of reproductive onset and success. *Nat. Genet.* **48**, 617–623 (2016).
39. P.-R. Loh, G. Tucker, B. K. Bulik-Sullivan, B. J. Vilhjálmsson, H. K. Finucane, R. M. Salem, D. I. Chasman, P. M. Ridker, B. M. Neale, B. Berger, N. Patterson, A. L. Price, Efficient Bayesian mixed-model analysis increases association power in large cohorts. *Nat. Genet.* **47**, 284–290 (2015).
40. P. Malik, N. Korfali, V. Srivastava, V. Lazou, D. G. Batrakou, N. Zuleger, D. M. Kananagh, G. S. Wilkie, M. W. Goldberg, E. C. Schirmer, Cell-specific and lamin-dependent targeting of novel transmembrane proteins in the nuclear envelope. *Cell. Mol. Life Sci.* **67**, 1353–1369 (2010).